2013-07-11

Popup Height and the Dynamics of Rising Buoyant Spheres

Randy H. Munns
Brigham Young University - Provo

Popup Height and the Dynamics of Rising Buoyant Spheres

Randy H. Munns

A thesis submitted to the faculty of
Brigham Young University
in partial fulfillment of the requirements for the degree of

Master of Science

Tadd T. Truscott, Chair
Scott L. Thomson
R. Daniel Maynes

Department of Mechanical Engineering

Brigham Young University

July 2013

ABSTRACT

Popup Height and the Dynamics of Rising Buoyant Spheres

Randy H. Munns
Department of Mechanical Engineering, BYU
Master of Science

In this paper the popup height of rising buoyant spheres is studied over a range of distinct release depths along with the accompanying velocities and accelerations near the free surface. In the past, regimes of motion due to vortex induced vibrations have been classified based on trajectories below the free surface. This study focuses on the popup height, velocity and acceleration at free surface exit, and vortex shedding in order to further define regimes of motion experienced by a rising buoyant sphere. Varying the release depth below the free surface reveals varying exit angles, velocities, accelerations, and popup heights at surface exit. Vortex shedding prior to free surface exit causes decelerations contributing to the variation in exit velocities and resulting popup heights. Using high-speed imaging and particle image velocimetry, we examine the trajectories, accelerations, velocities and vortex shedding events for spheres of different mass ratios over a range of Reynolds number (2×10^4 Re 6×10^5). At lower Re, spheres released from shallow release depths result in greater accelerations and velocities at free surface exit along with greater popup heights compared to releases from deeper depths. After reaching a depth which results in a minimum popup height, further increasing the release depth reveals an increase in popup height demonstrating an oscillatory pattern due to the sphere being released from vortex forces after shedding. This pattern is repeated as the popup height again decreases with greater release depths. For spheres of greater Re, popup height increases linearly with release depth, demonstrating continued accelerations at free surface exit.

Keywords: popup, oblique, oscillating, free surface, trajectory, vortex

ACKNOWLEDGMENTS

I would like to personally thank Dr. Tadd Truscott for his guidance and help throughout this work. I would also like to thank the members of the Splash Lab for help with long lasting experiments. I personally thank my wife Lindsay for her love and support and also my children Kylee and Cooper.

This material is based upon work supported by the National Science Foundation under Grant No. CMMI-1126862. Any opinions, findings, and conclusions or recommendations expressed in this material are those of the author(s) and do not necessarily reflect the views of the National Science Foundation.

TABLE OF CONTENTS

LIST OF TABLES . . . . . **v**

LIST OF FIGURES . . . . . **vi**

NOMENCLATURE . . . . . **vii**

Chapter 1 Introduction **1**
1.1 Past Research 4
1.2 Force Balance 5

Chapter 2 Methods **8**
2.1 Experimental Setup 8
2.2 Experimental Considerations 10

Chapter 3 Results **16**
3.1 Regimes of Motion 16
3.2 Popup Height 17
3.3 Trajectories 25
3.4 Vortex Shedding 33
3.5 *Re* at Free Surface Exit 40
3.6 Low *Re* 42

Chapter 4 Conclusion **43**

REFERENCES **45**

LIST OF TABLES

2.1 Experimental process for each sphere 8
2.2 Physical characteristics of spheres 10

LIST OF FIGURES

1.1 Trajectories and popup for different release depths 2
1.2 *Re* of past research 3
1.3 Free body diagram of a rising buoyant sphere 5

2.1 Experimental setup 9
2.2 Experimental setup: PIV 11
2.3 Time series of ensemble averaged vector fields of settling particles 12
2.4 Velocity of particles in tank versus time 13

3.1 Image sequence of an ascending 3 inch sphere from four different release depths . . 17
3.2 Popup height versus release depth normalized by diameter for 4 spheres 18
3.3 Velocity at free surface exit versus release depth 20
3.4 Acceleration at free surface exit versus release depth 21
3.5 Still images of popup event with popup data for ping pong ball 22
3.6 Isometric view of 3D trajectories of ascending spheres in water 25
3.7 Trajectories from 3 release depths in the x-y and z-y planes 27
3.8 Trajectory plotted as radial deviation *R* in the accelerating regime 29
3.9 Trajectory plotted as radial deviation *R* in the oscillatory regime 30
3.10 Trajectory plotted as radial deviation *R* in the oscillatory regime: deeper release . . 31
3.11 Overlay of radial deviation normalized to a single release depth 32
3.12 PIV vector fields in accelerating regime 34
3.13 PIV vector fields in accelerating regime for SS6 35
3.14 PIV vector fields in oblique regime 37
3.15 PIV vector fields in oscillatory regime 37
3.16 Still image of popup event at apex with accompanying plume from vortex 38
3.17 PIV vector fields in oscillatory regime 39
3.18 *Re* vs popup height 41

NOMENCLATURE

breach	Top of sphere entering the air water interface known as the free surface
D	Diameter of a sphere
h_d/D	Release depth of a sphere below the free surface, normalized by diameter
h_p/D	Popup height of a sphere above the free surface, normalized by diameter
PP	Abbreviation for pingpong ball
SS3	Abbreviation for stainless stee sphere: nominal diameter of 3 inches
SS4	Abbreviation for stainless stee sphere: nominal diameter of 4 inches
SS6	Abbreviation for stainless stee sphere: nominal diameter of 6 inches
ψ	Sphericity of an object or particle

CHAPTER 1. INTRODUCTION

Anyone who has taken a buoyant ball into a swimming pool has inevitably pulled the ball under the surface and released it. After release the ball rises quickly up through and above the free surface (i.e. popup). Counter to popular thought or intuition, a shallow release depth results in a greater maximum popup height when compared to a deeper release depth. Bourrier [1] observed this same phenomenon while studying the underwater trajectory of rising spheres which led him to classify different regimes of motion — accelerating, transitional, and vortex (oscillatory) — below the free surface based on varying trajectories and popup heights.

Objects that interact with the free surface employing forces of buoyancy and/or propulsion are found all around the world. Breaching animals pop up above the free surface for various purposes. Penguins in particular exit the water propelling themselves onto icebergs to return home after a hunt and avoid predators. Using bubbles during ascension in order to reduce drag and increase exit velocity, emperor penguins are able to pop up out of the water at great heights [2]. Great white sharks breach the free surface using several predatory maneuvers exiting the water either completely or partially. When complete exit is achieved the shark can pop up such that the entire body is as much as three meters above the surface of the water [3]. Whales breach the free surface jumping so that most of the body is clear of the water [4]. Dolphins interact with the free surface during travel and social behavior, leaping completely out of the water before a dive [5].

Submarines surface after months in the depths of the ocean. On occasion, an emergency requires quick surfacing maneuvers where the nose of the submarine is pointed up and the bladders are emptied with high pressure air. The submarine then ascends to the top using buoyancy as the driving force [6]. Certain classes of missiles have been designed to launch from submarines and be propelled with such an initial velocity to cause the missile to breach the free surface and travel up into the atmosphere, where the primary rocket motor ignites [7].

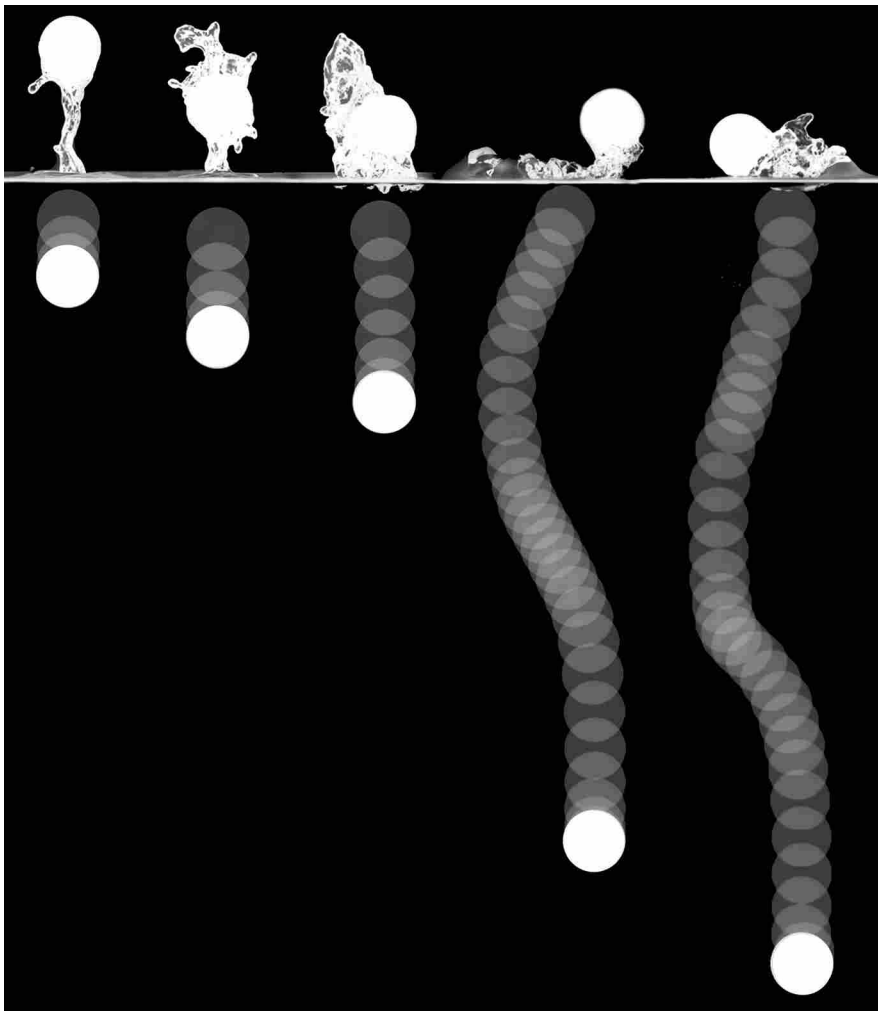

Figure 1.1: Images of maximum popup heights (h_p/D) above the free surface for spheres released from varying depths. The release depth (h_d/D) for each case increases from left to right (h_d/D: 1,2,3,10,12, h_p/D: 2.7,1.6,1.4,1.4,1.0). Trajectories are shown below the free surface as superimposed transparent images 20 ms apart. Each sphere (ping pong ball) was released from rest following a 15 minute settling time.

Spheres represent, perhaps, the most canonical type of object rising to and exiting the surface. Driven to the surface only by a buoyant force, the behavior is unique. Prior to breach and exit of the free surface, an ascending sphere may experience a non-vertical trajectory depending on the release depth (see Figure 1.1). Figure 1.1 illustrates the trajectory of a sphere released from different release depths along with the associated velocities and accelerations during ascension. The deviation from a completely vertical trajectory seen in the two trajectories on the right is due to vortex induced vibrations. The ascending sphere experiences traditional wake formation, detach-

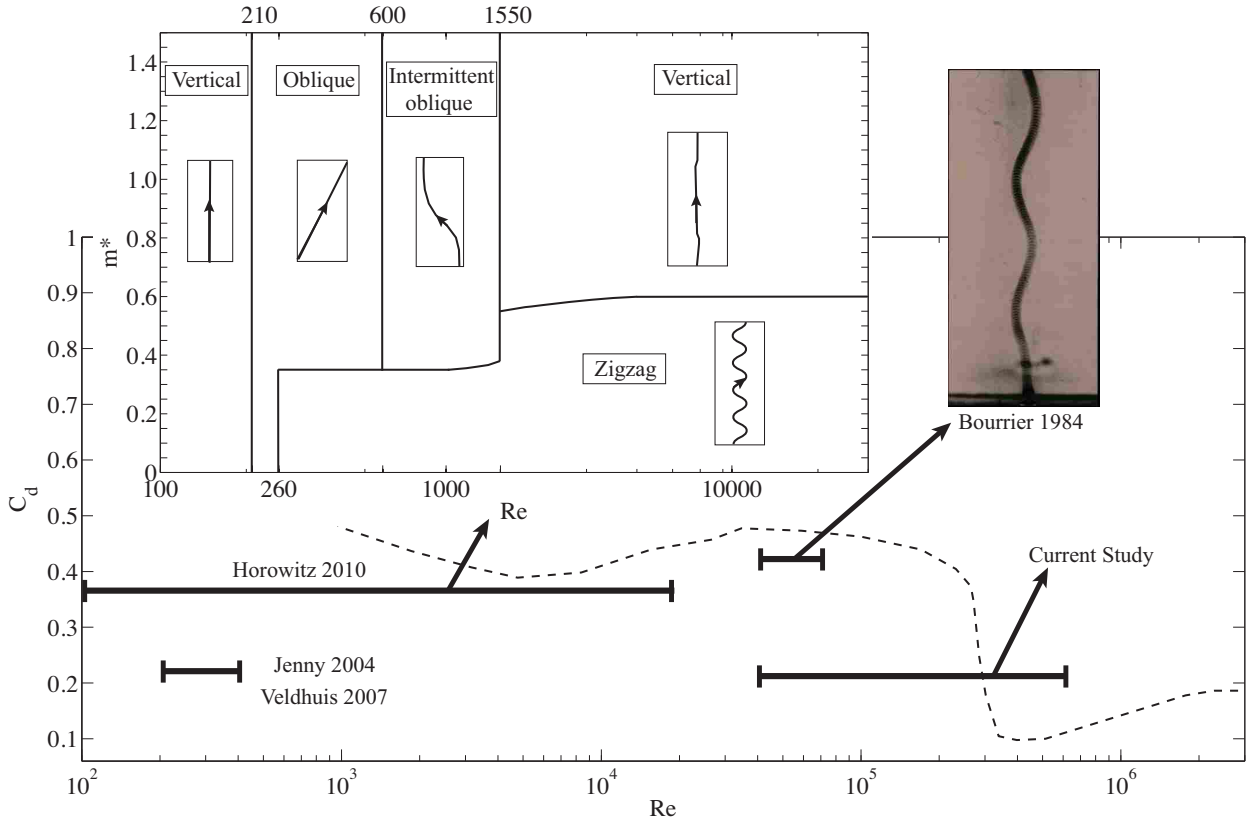

Figure 1.2: Ranges of Re studied by scientists for rising spheres shown as dark lines. The range of *Re* covered in the current study is also shown. The dashed line is the standard C_d versus *Re* curve and the lines are the extent of each study in *Re* only. Inset plot redrawn after Horowitz et al. [8].

ment and vortex shedding due to skin friction and boundary layer effects. When released from rest, the sphere accelerates with axisymmetric wake formation which transitions to periodic shedding as the Reynolds number (*Re*) increases. Periodic vortex shedding in the wake induces an imbalance of horizontal forces on the sphere resulting in an oscillatory trajectory during ascension. Depending on the release depth below the free surface, the vortices change size and position relative to the sphere before breach and exit, varying the trajectory of the sphere along with the maximum popup height (Figure 1.1 far right). Surprisingly, not all spheres will pop up and leave the free surface. Smaller diameter spheres with low *Re* will not develop enough momentum to rise above the free surface. This is due to forces of momentum and buoyancy being overcome by the forces of drag.

1.1 Past Research

Since Newton's reports of a nonlinear trajectory caused by periodic wake shedding by studying free falling particles from the dome of St. Paul's Cathedral [9], numerous experimental and numerical investigations have provided quantitative and qualitative explanation of paths and trajectories under the free surface of freely rising (and falling) spheres, along with the wakes and accompanying vortex structures which are summarized here and in Figure 1.2. While observing spheres rising in a free fluid and the noticeable difference in popup modes at the free surface, Bourrier et al. [1] reported the existence of two regimes of motion, defined as accelerating and vortex (oscillatory) regimes, separated by a transition regime. We note that Bourrier's work was performed at 40,000$<$ *Re* $<$90,000. The drag coefficient (C_d) for free rising spheres was studied experimentally by Karamanev et al. and [10] he reported a deviation from the standard drag curve for spheres with $Re > 3000$. His results showed the existence of two different regimes of rising spheres: rectilinear and spiral regimes which showed the frequency of the spiral wavelength (Strouhal number *St*) of light rising spheres to be constant and independent of *Re* (225$<$ *Re* $<$100,000) [11]. Regimes have been further quantified through numerical simulations on both rising and falling spheres by Jenny et al. [12] and confirmed experimentally by Veldhuis [13] (225$<$ *Re* $<$550). These reported regimes include: vertical acceleration, rectilinear steady oblique, oscillatory-oblique, zigzag (oscillatory) and chaotic. Critical mass ratios were found and reported by Horowitz showing that not all buoyant spheres will oscillate ($100 >$ *Re* $>$20,000) [8]. The onset of oscillation sets in earlier for light spheres than for dense ones [12], which we have confirmed through our experiments.

While the dynamics of motion and wake formation of buoyant spheres has received considerable attention in the last 20 years, past studies have focused on low *Re* and neglected the physics of the popup. Figure 1.2 shows ranges of *Re* in the studies of past researchers as well as the *Re* to be studied in the current research. The inset plot in Figure 1.2 is redrawn after Horowitz et al [8] and defines regimes — acceleration, transition, and zigzag — and the accompanying trajectory based on mass ratio (m^*) and *Re*. Where past researchers have covered *Re* below 3×10^4, the present study will be experimenting on *Re* ranging between 2×10^4 and 6×10^5.

While the nomenclature of the regimes of a rising buoyant sphere varies in the literature, the actual behavior does not. All researchers seem to agree upon the following sequence: an initial

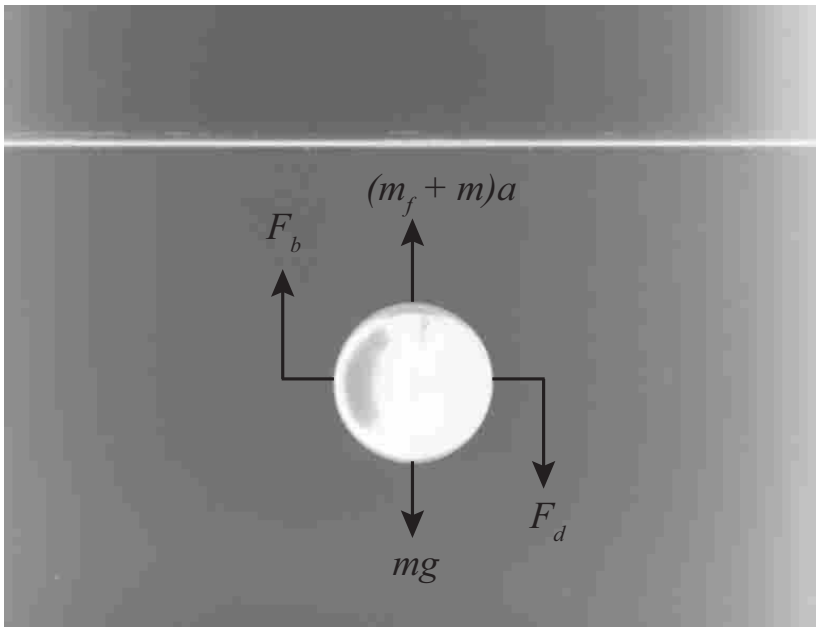

Figure 1.3: Free body diagram of a rising buoyant sphere.

accelerating regime (vertical), followed by a transition regime (oblique) and a final oscillatory (zigzag) regime. Where Jenny et al. [12] and Veldhuis et al. [13] report a final chaotic stage following the oscillatory regime, Horowitz reports that any chaotic behavior is due to lack of quiescence in the fluid before sequential releases which also contributes to any motion of the sphere outside of a 2-D plane [8]. This claim by Horowitz was taken into account in the presently described study through a quiescence analysis using PIV.

1.2 Force Balance

The interaction of any blunt object with fluid can be described by the forces and torques induced by motion of the object through the fluid. "These hydrodynamical efforts include added inertia (also often referred to as added mass) contributions resulting from the instantaneous reaction of the fluid to a body displacement (translation and/or rotation), which are determined entirely by the body shape and do not depend on the vorticity generated at its surface, nor on that which may eventually exist in the core of the fluid" [14]. The extra term of added mass becomes a function of time and position as the sphere breaches and exits the free surface and is always coupled with an acceleration term.

The ascension of a rising buoyant sphere is modeled with a simple theoretical force balance illustrated in Figure 1.3 and demonstrated as follows

$$\begin{aligned} ma + m_f a &= F_b - mg + F_d \\ ma + m_f a &= F_b - mg + 1/2\rho A C_d(Re) V^2, \end{aligned} \tag{1.1}$$

where m is the mass of the sphere, m_f is the added mass ($2/3\pi R^3 \rho_f$), a is the acceleration, F_b is the buoyancy force, F_d is the drag force, A is the cross sectional area, $C_d(Re)$ is the coefficient of drag at the given Reynolds number, and V is the velocity of the sphere. Solving the force balance for velocity yields,

$$V = \sqrt{\frac{F_b - mg - ma - m_f a}{1/2\rho A C_d(Re)}}, \tag{1.2}$$

and assuming terminal velocity removes any acceleration terms and yields,

$$V = \sqrt{\frac{F_b - mg}{1/2\rho A C_d(Re)}}. \tag{1.3}$$

In order to predict popup height above the free surface, an energy balance of potential (at the max popup) and kinetic (at exit) energy yields

$$\begin{aligned} mgh_p &= 1/2 m V^2 \\ h_p &= \frac{V^2}{2g}, \end{aligned} \tag{1.4}$$

where h_p is the maximum popup height, V is terminal velocity from equation 1.3.

In this paper the popup height above the free surface of a rising buoyant sphere will be examined experimentally and correllated with release depth. Spheres of varying diameters and materials will be released from varying depths and allowed to popup. Behavior of the trajectory of a sphere will be examined during ascension and breach of the free surface in order to discuss regime classification based soley on physical paths. In order to futher regime definition, accelerations and velocities will be examined at free surface exit through the use of high speed imaging. Exploration of the physics and dynamics behind the trajectory and popup of a sphere through 2D PIV will be

performed. Visualization of vortex structures forming and detaching from an ascending sphere will be presented and correlated with the resulting accelerations, velocities and popup heights. Finally, *Re* will be calculated at the free surface in order to determine *Re* dependence on popup height and compare with a simple force balance and theoretical model.

CHAPTER 2. METHODS

2.1 Experimental Setup

In order to determine the maximum pop up height above the free surface and track the sphere trajectory below, high-speed cameras were used to image the ascent from release to the apex of the popup for four different spheres of varying mass ratios (ρ_s/ρ_f) and diameter. The sphere was set to a specified depth in the center of a tank filled with water. After a sufficient wait time to allow the water to become quiescent, the sphere was released and imaged during ascension, breach, exit of the free surface, and apex of the trajectory above the fluid. The sphere was then set again at the desired depth and the water allowed to settle for the next release. In order to produce a meaningful statistical sample, ten iterations were performed at each release depth. Release depths were incremented in half diameters of the respective sphere, as measured from the free surface to the top of the sphere, up to a depth of approximately ten diameters. Table 2.1 shows the experimental information for each case.

The setup of the cameras, tank and light banks are illustrated in Figure 2.1. Two cameras were placed 90° apart from each other, perpendicular to the tank. Fluorescent light banks were

Table 2.1: Experimental process for each sphere. Release depths increment in half diameters measured from the free surface to the top of the sphere.
PP: pingpong ball, SS: stainless steel.

Sphere	Diameter cm (in)	Release depths D	# releases at each depth
PP	4 (1.57)	0.5-12	10
SS3	7.62 (3)	0.5-10	10
SS4	10.16 (4)	0.5-10	10
SS6	14.92 (6)	0.5-6	2

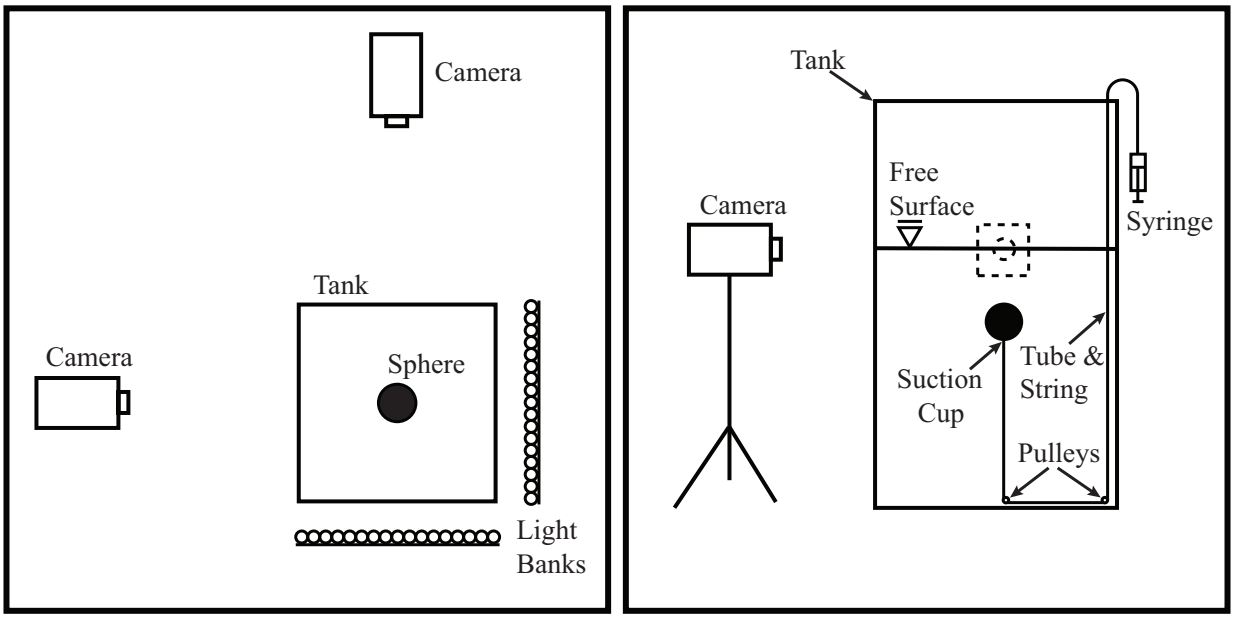

(a) top view (b) side view

Figure 2.1: Experimental setup with cameras, tank, and light bank.

used as backlighting in order to increase contrast. Consistent release depths were controlled by a pulley clutch system with a laser level marking the top of the sphere. The spheres were submerged, held in place, and released using a suction cup, tube and syringe to create a vacuum. The glass tank used for all experiments of high speed imaging and PIV was 81.3 cm$\times$81.3 cm$\times$182.9 cm and held approximately 806 L of water. High speed cameras (Photron FastCam SA-3) were used to record the ascension and popup of the rising spheres. Images were recorded at 1000 frames per second (fps) with a resolution of 1024$\times$1024 pixels for the popup images and 512$\times$1024 for the full trajectories from release to free surface exit. The field of view for the popup images was 52 cm$\times$52 cm, yielding a 19.7 pixels$\cdot$cm^{-1} magnification, and 47 cm$\times$94 cm, yielding a 10.9 pixels$\cdot$cm^{-1} magnification for the trajectory images (underwater). For the popup images, data was recorded of the ascension of the sphere, as the sphere entered the field of view just below the free surface to the apex of the ascent above the free surface. The entire trajectory was also recorded from each release depth to free surface exit.

The physical characteristics and parameters of the spheres used in this study are shown in Table 2.2. Four separate spheres were chosen of differing diameters in order to span values of

Table 2.2: Physical characteristics of spheres. Center of mass is reported as distance of center of mass from the geometric center.

Sphere	Mass ratio	Diameter cm (in)	*Re*	Sphericity	Center of Mass μm	Roughness r.m.s. $\pm\mu$m
PP	0.08	4 (1.57)	2.12e5	98.9±1.1%	96.2±25	4.10±.06
SS3	0.35	7.62 (3)	2.96e5	97.0±1.2%	41.8±3.6	0.40±.08
SS4	0.31	10.16 (4)	4.68e5	97.9±.65%	624.3±36	0.37±.03
SS6	0.28	14.92 (6)	8.50e5	98.6±.37%	294.5±18	0.29±.01

Reynold's number (*Re*) that include laminar and turbulent regimes. *Re* for these spheres range between 5×10^4 and 6×10^5, calculated using terminal velocity of thr respective spheres. Past researchers have covered *Re* below 5×10^4. The stainless steel (SS) spheres used were hollow and of nominal diameters: 3, 4, and 6 inches (7.62, 10.16, 14.92 cm), and will be referred to as SS3, SS4, and SS6, respectively. The pingpong ball used is a standard ping pong ball of 4 cm (1.57 in) diameter. Mass ratio is defined as $m^* = \rho_s/\rho_f$.

2.2 Experimental Considerations

One experimental consideration which presents itself throughout the literature is an adequate wait time in between experimental releases for the water in the tank to become quiescent. Horowitz and Williamson [8] claim a wait time of 2 hours in between experimental runs (sphere releases) to ensure quiescence. They show through experimentation that a sphere released after a 2 hour period will result in a trajectory where the sphere will ascend in a single plane with no helical or 3D path. Other scientists and researchers have run experiments involving wait times of 5-30 minutes in between releases. These researchers do not claim quiescence nor non-oscillatory motion of the sphere as do Horowitz and Williamson. Quiescence is desirable before each release to provide consistent experimental conditions. Were experiments performed with residual fluid motion the behavior of the spheres becomes much less consistent. Therefore, the wait time for quiescent conditions is an important factor when realizing that there are over 400 individual releases to be performed throughout the present study. A method for determining an adequate wait time to quiescence for experiments involved in the current study is presented here.

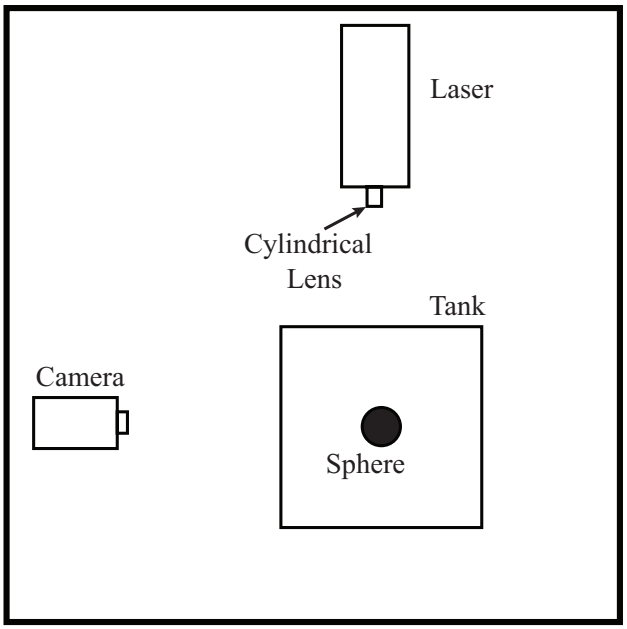

Figure 2.2: Setup for capturing PIV images to be post processed. The cylindrical lens forms a sheet from the laser beam.

Particle image velocimetry (PIV) was used to determine quiescence in the tank. The water in the tank was densely seeded with polyamide seeding particles with a density of ρ_p = 1030 kg/m^3, and nominal diameter of 50 μm ($\pm$ 20 μm). A Quantronix Darwin Duo YLF 527 nm laser was pulsed at 1000 Hz to illuminate the seeding particles while a Photron SA3 high speed camera captured images at a time step of 1 frame per second (FPS) and a resolution of 768 $\times$ 768 pixels for the ping pong ball, and 1024 $\times$ 1024 pixels for the other spheres. The field of view for the pingpong ball was 21.3 cm $\times$ 21.3 cm, and 33.2 cm $\times$ 33.2 cm for the other spheres, yielding magnifications of 36 pixels cm^{-1} and 30 pixels cm^{-1} respectively. A pulse generator was used as an external trigger for both the camera and the laser. Following an experimental run and resetting of the sphere, images were captured every five minutes for one hour. At each five minute interval, with time zero ($t = 0$) being the reset of the sphere, the laser and camera were triggered for approximately 30 seconds capturing 30 images.

PIV was performed using the open source code MATPIV. Since the flow velocities vary from high at release ($t = 0$), to zero at quiescence, three time steps (dt values of 1, 5, and 10 seconds) were used in order to ensure sufficient temporal resolution, i.e., a 5 or 10 second dt

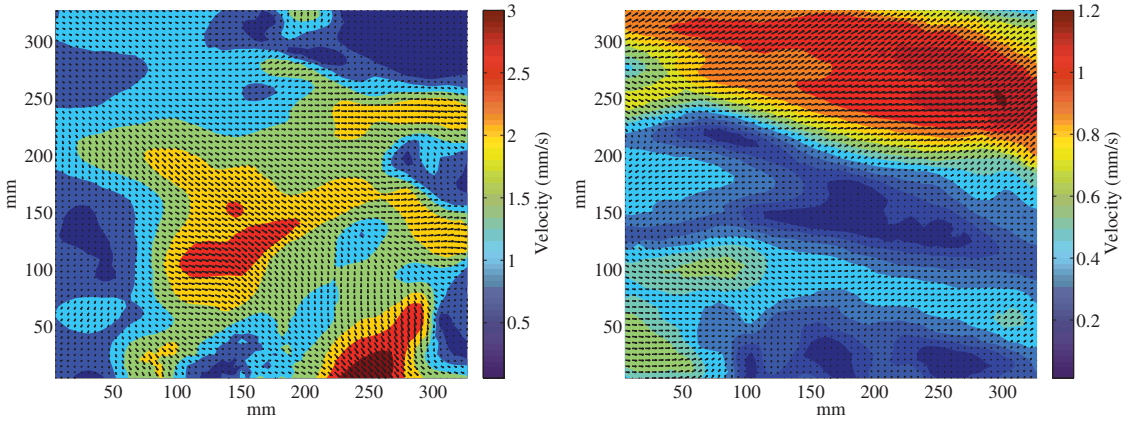

(a) $t = 0$ min (b) $t = 10$ min

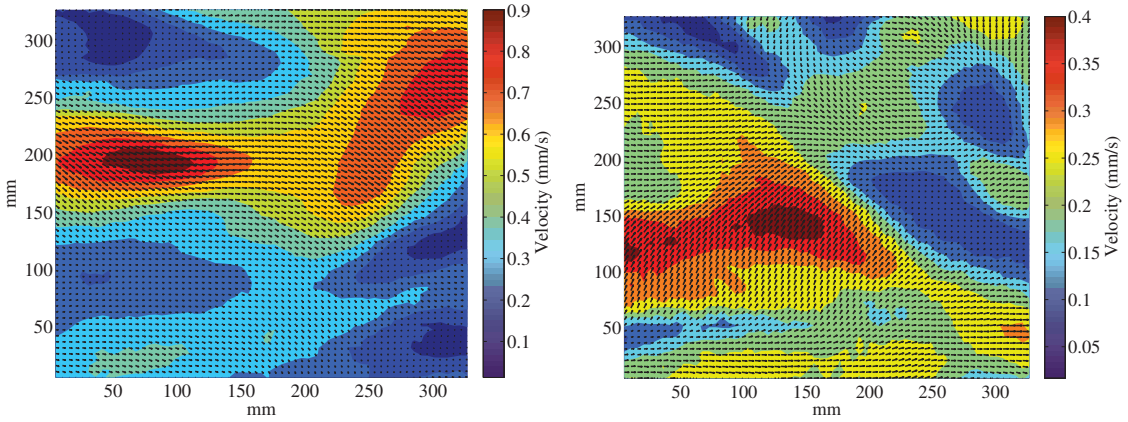

(c) $t = 20$ min (d) $t = 30$ min

Figure 2.3: Time series of ensemble averaged vector field plot of the stainless steel 3 inch sphere. The vector fields shown use $dt = 1$ with an ensembled average of 20 vector fields at each interval.

will show very good results as the flow tends toward quiescence and poorer results when the flow velocity is greatest at t = 0. For each 5 minute interval, 20 pairs of images were processed and correlated using all three dt time steps. Ensemble averaged vector fields at time intervals of 0, 10, 20, and 30 minutes and a time step of dt = 1 second are shown for the SS3 sphere in Figure 2.3. Each vector field is an ensemble average of 20 individual vector fields. The flow shows much higher velocities in Figure 2.3a because the sphere has just been released and reset. The flow becomes more still with time as the velocity scales decrease significantly in Figure 2.3d after waiting 30 minutes.

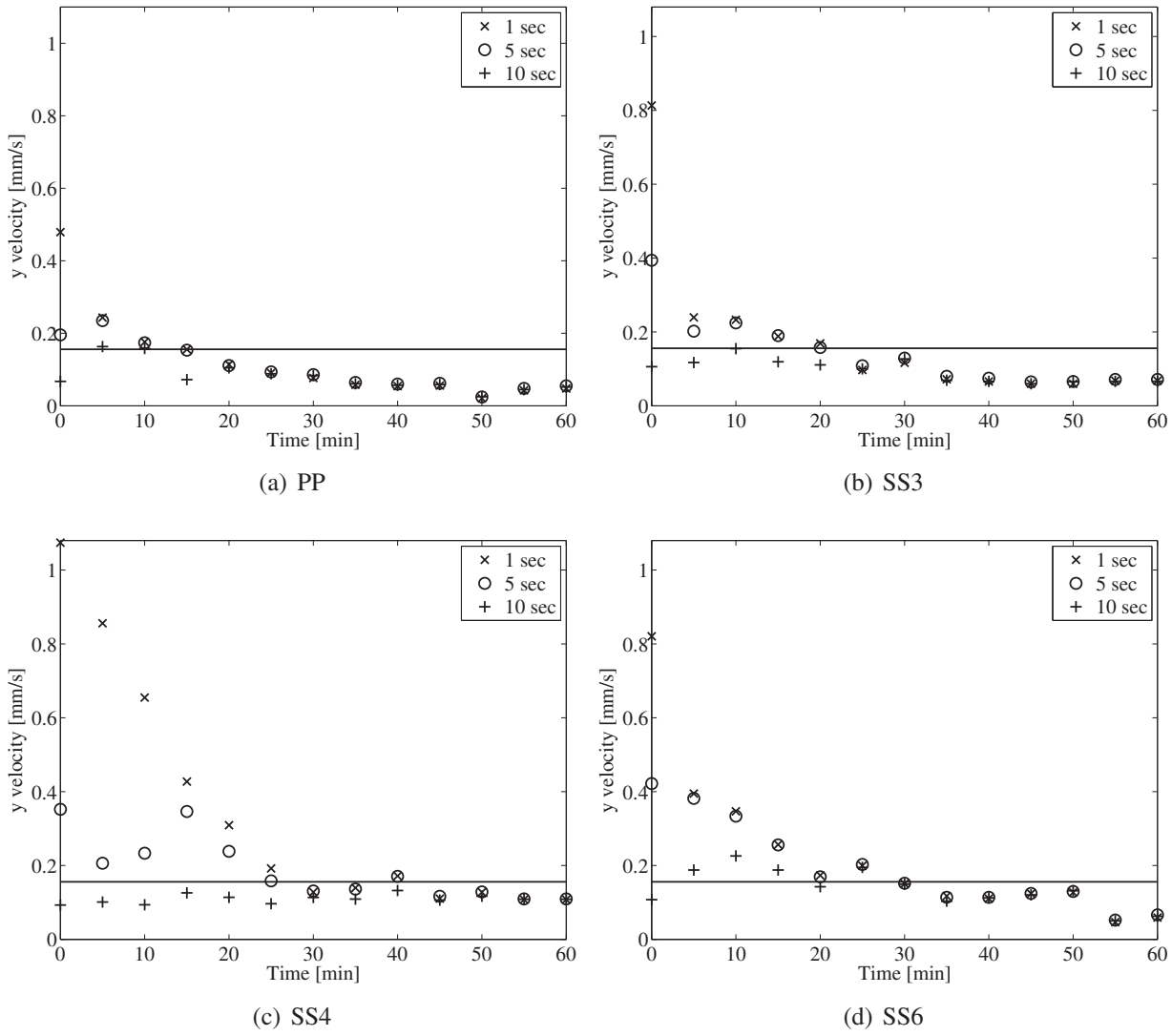

(a) PP (b) SS3

(c) SS4 (d) SS6

Figure 2.4: Velocity of particles in tank versus time. At $t = 0$, the sphere has been reset in the tank directly after being released from 10 diameters below the free surface. Legend refers to dt spacing between image pairs to ensure that poor temporal resolution was not responsible for lowered velocity values. The settling velocity (U_∞) for the polyamide seeding particles is also plotted as a solid line.

Figure 2.4 shows the temporal average of the ensemble averaged vector fields for all spheres at each time step and 5 minute interval from 0-60 minutes, i.e., calculating the average velocity magnitude (single value) for each ensemble averaged vector field. The settling velocity for the polyamide seeding particles is also plotted as a solid line. After performing a force balance analysis on a single seeding particle, the particle settling velocity was calculated using

$$U_\infty = \frac{2(\rho_p - \rho_f)a^2 g}{9\mu}, \tag{2.1}$$

where U_∞ is the settling velocity of a single particle suspended in water, ρ_p is the density of the particle, ρ_f is the density of the fluid, a is the radius of the particle, g is the gravitational constant, and μ is the dynamic viscosity of the fluid. Taking into consideration the size distribution of the seeding particles (50 μm $\pm$ 20 μm) the settling velocity varies from 0.3052 to 0.0561 mm/s, with the average being 0.1557 mm/s. The settling velocity was calculated as 0.1557 mm/s for a nominal particle diameter of 50 μm. These calculations and data indicate that a 15 minute wait time for the ping pong ball and a 30 minute wait time for the other three spheres will be sufficient for the fluid to become quiescent and was implemented herein.

The sphericity has been calculated and reported in order to show the roundness of each of the spheres used in the present study. According to Wadell [15], the sphericity of an object (or particle) is the ratio of the surface area of a sphere of the same volume as the particle divided by the actual surface area of the particle. The expression used to calculate the sphericity of any object is

$$\psi = \frac{\pi^{1/3}(6V_p)^{2/3}}{A_p}, \tag{2.2}$$

where ψ is sphericity, V_p is the volume of the particle, and A_p is the surface area of the particle. Sphericity gives a sense of the deviation of the actual measured diameter from the nominal diameter of a ball. An ideal sphere would have the sphericity of ψ = 1, or 100% sphericity. Sphericity measurements are reported in Table 2.2. All 4 spheres show high sphericity which will result in constant experimental conditions.

Jenny et al. [12] showed that induced motion (i.e., oblique oscillating rather than oblique steady, or chaotic rather than oscillatory) could be initiated with a nonhomogeneous sphere. This was accomplished in numerical simulations by adding a small imperfection to the model that pro-

duced a center of mass that was initially horizontal with the geometric center, resulting in an initial rotation [12]. For the spheres used in this study, center of mass was determined by placing a sphere in a bucket of water. Soap was added to the water in order to reduce the effects of surface tension. After releasing each sphere 10 times from an arbitrary position and allowing it to rotate and settle, the top of the sphere was marked with an 'x'. At this settled position the assumption was made that the center of mass was located along the static vertical axis. The spheres were then released a second time with the pole of the center of mass positioned 90° from vertical, horizontal with the geometric center. The angular rotation was recorded using high speed imaging and the time spanning 90° of travel was calculated from the images. This second release was performed and recorded for 5 iterations. The sphere was then modeled as a pendulum beginning at a horizontal position. A first order approximation was derived expressing the distance separating the geometric center and the center of mass as a function of time as follows

$$\begin{aligned} l &= \frac{I\alpha}{mg} \\ &= \frac{\pi r^2}{3gt^2}, \end{aligned} \tag{2.3}$$

where I is the mass moment of inertia of a sphere, α is the angular acceleration of the sphere, m is the mass of the sphere, g is the gravitational constant, r is the radius of the sphere, and t is the time span of 90° of rotation. The deviation of the center of mass from the geometric center is reported for each sphere in Table 2.2. These calculations show that the spheres are susceptible to induced motion as described by Jenny et al. [12]. In order to reduce bias in the experimental results, and with the unability to completely remove the tendency of the ball to rotate, orientation of the sphere at release was selected at random.

Roughness of the spheres was determined after the manner reported by Truscott [16]. The length of the path was 4.8 mm and averaged RMS values are reported in Table 2.2.

CHAPTER 3. RESULTS

This section includes presentation and discussion of results for the experimental runs in Table 2.1 and the data accumulated for the spheres in Table 2.2. Each release was performed after a specified wait time for quiescence of the fluid in the tank as determined in Section 2.2. A brief discussion is presented of possible regimes of motion experienced by an ascending buoyant sphere. Popup height, results are presented and discussed along with acceleration and velocities at the free surface. A discussion on regimes will be presented based on popup height correlated with acceleration and velocities at free surface exit. Trajectories will be shown in order to compare and further regime definition and classification of rising spheres based on popup height, acceleration and velocity at free surface exit. Visualization of vortex shedding through PIV will be presented in order to show correlations between the accelerations, velocities, popup height and the shedding event. Finally, calculations of *Re* will be examined and correlated with popup height data along with a simple theoretical model and force balance predicting popup height and exit velocities.

3.1 Regimes of Motion

Presentation of data and results throughout this section will be correlated with regimes of motion experienced by a rising buoyant sphere. Three regimes will be used to describe the ascent of the spheres in this paper: accelerating, oblique, and oscillatory. The accelerating regime is defined by a completely vertical trajectory with no deviation in the horizontal direction and has not yet reached terminal velocity as seen in Figure 1.1. The oblique regime follows the accelerating regime and is defined by a slight angle in the vertical trajectory during ascension. The oblique regime is a transition between the accelerating and final oscillatory regime. Spheres ascending in the oscillatory regime follow a periodic oscillating trajectory which is vertical in the mean and it is assumed that terminal velocity has been reached. When a sphere approaches a turn in the oscillatory path, the velocity decreases as the sphere rounds the corner and changes direction.

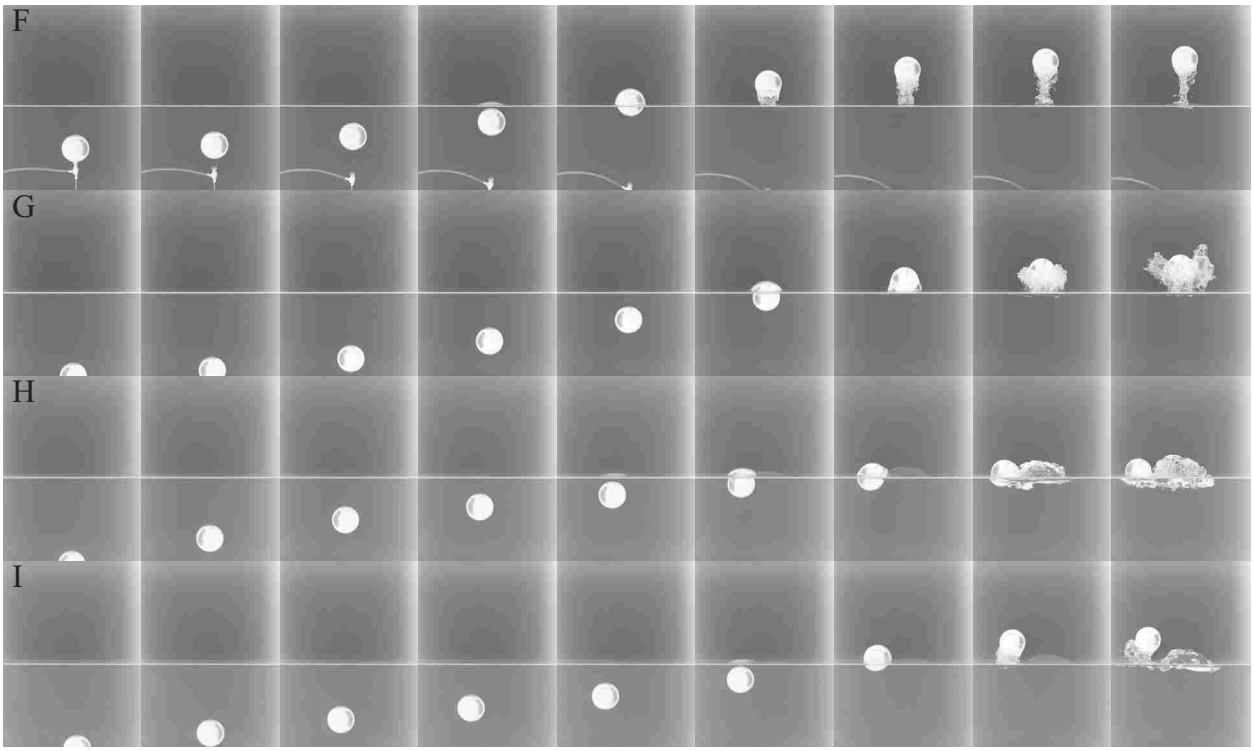

Figure 3.1: Image sequence of an ascending 3 inch Stainless Steel (SS3) sphere from four different release depths: h_d/D = 1, 2.5, 5, 6.5 (from top to bottom). The images were captured at 1000 fps. The far right image depicts the maximum height or apex for the individual time series and respective release depths. The maximum popup heights are: h_p/D = 2.25, 1.51, 0.98, 1.27 (from top to bottom). The time step between images in each time series is as follows from top to bottom: dt = 39, 41, 51, 59 ms.

After the switch back has been completed, the velocity increases until the next turn in the path is approached.

3.2 Popup Height

In the spirit of Bourrier's et al. [1] work of defining regimes of buoyant rising spheres through observing varying popup heights above the free surface, popup heights of four different spheres were imaged using high speed cameras. Figure 3.1 shows high speed images of a time series for an ascending 3 inch Stainless Steel (SS3) sphere from four different release depths: h_d/D = 1, 2.5, 5, 6.5 (from top to bottom). In each time series at the far left, the sphere is begins at the center of the frame during ascension. Upon breach and exit of the free surface, cases F and G

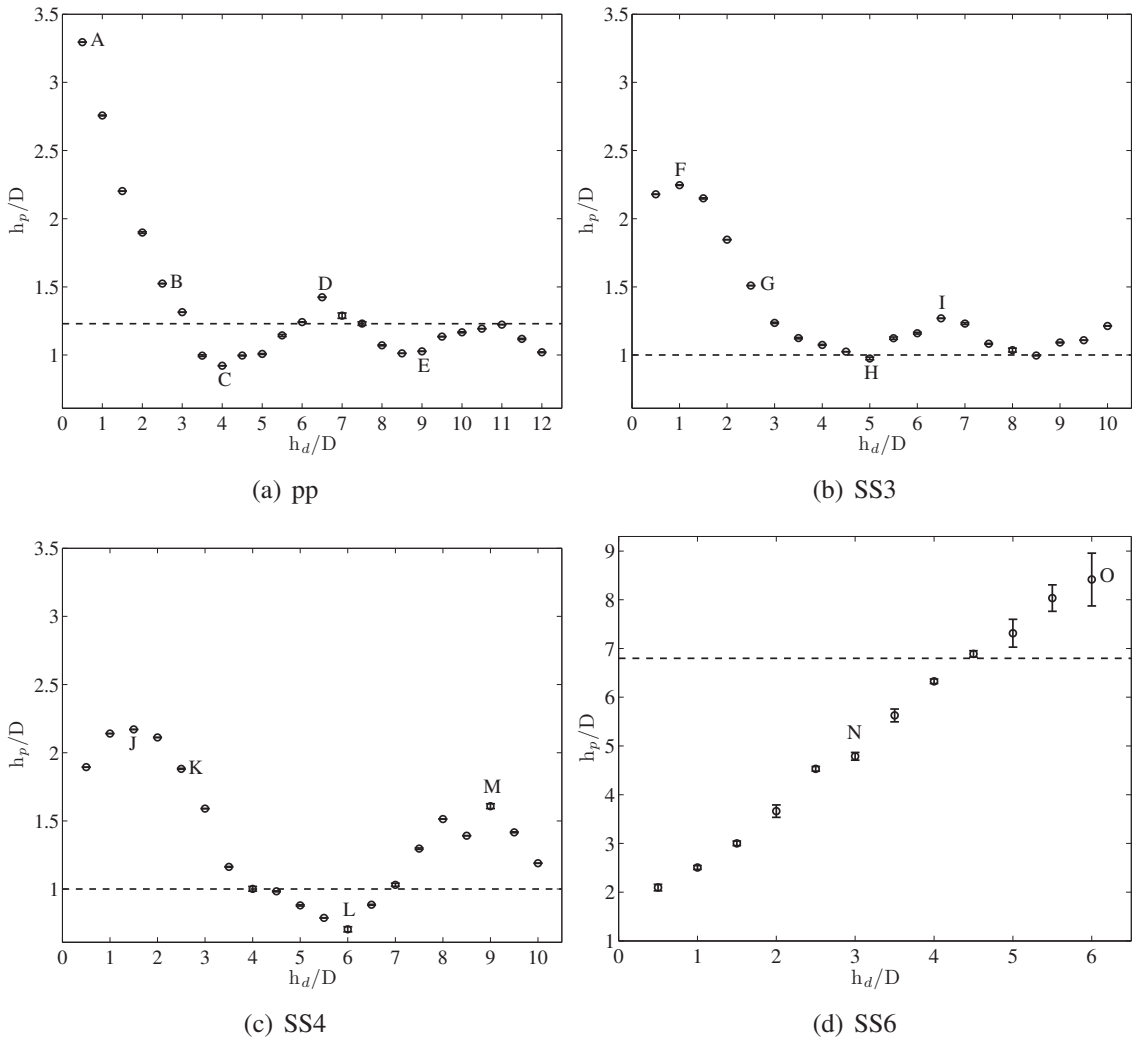

(a) pp (b) SS3

(c) SS4 (d) SS6

Figure 3.2: Popup height (h_p) versus release depth (h_d) normalized by respective diameter (D) for all 4 cases in the present study. The error bars are reported with a 95% confidence interval on the mean using a students-t distribution based on 10 runs for a-c and 2 runs for d. The horizontal dotted line represents the predicted maximum popup height, as discussed in section 1.2.

shown in Figure 3.1 remain in the center of the frame whereas the cases H and I deviate from the center of the frame. The splash curtain at the free surface is different for each case along with the maximum popup height magnitude above the free surface: h_p/D = 2.25,1.51, 0.98, 1.27 (from top to bottom).

Data extraction from the raw high speed images was realized through image processing of the trajectory and popup event. Processing techniques take into account the motion of the sphere within the frame which required tracking the relative diameter of the sphere in each individual run.

Distance above the free surface, popup height (h_p), was normalized by the relative diameter (D) of the sphere in pixels for each run. Popup height magnitudes are reported as normalized values h_p/D compared to normalized release depths h_d/D.

Data extracted from the images are presented in Figure 3.2 and show the distribution of popup height (h_p/D) versus release depth (h_d/D) for each of the spheres in the present study. The error bars are reported with a 95% confidence interval on the mean using a students-t distribution based on 10 runs at each depth for Figure 3.2a-c and 2 runs at each depth for Figure 3.2d. The very small nature of error bars displayed in the plots demonstrates the repeatability of these experiments. The horizontal dotted line shows the predicted maximum popup height based on a simple force balance which is much lower than the actual maximum popup height. This difference can be attributed to the fact that the sphere is actually accelerating while exiting the free surface (more discussion is made in Section 3.5).

The general curve of the popup data in Figures 3.2a-c reveal a sinusoidal-like, oscillating pattern. The maximum popup heights for Figure 3.2a-c were reached when the sphere was released from a shallow release depth: h_d/D = 0.5, 1, 1.5 for the pingpong, SS3 and SS4 spheres respectively. The maximum heights reached are shown as cases A, F, and J. As the release depth increases, the popup height decreases until the data reach a valley or local minimum where the lowest popup heights occur when the sphere is released from deeper depths: h_d/D = [4, 8.5, 12],[5, 8.5],[6] for the pingpong, SS3 and SS4 spheres respectively, shown at cases C, H, and L. Following occurrence of the lowest popup heights, increased release depths reveal increasing popup heights resulting in another peak or local maximum popup height at h_d/D = [6.5, 11],[6.5],[9] at cases D, I, and M. Popup height of the local maximum peak from a greater release depth never reaches the same magnitude as the maximum popup height from a shallow release depth. The SS4 case, Figures 3.2c, shows the most narrow difference in magnitude between the two peaks, 0.563 D. The pingpong ball case, Figures 3.2a, shows the greatest difference in magnitude, 1.871 D. This pattern is repeated with peaks and valleys as the release depth increases.

Popup height above the free surface is dependent on velocity and acceleration of the sphere at free surface exit. After reaching terminal velocity, vortices begin to form and shed in the wake, altering the trajectory and speed of the sphere (see Figure 1.1). These vortex induced vibrations are the cause of accelerations and decelerations illustrated in Figure 1.1. Vortices form and shed

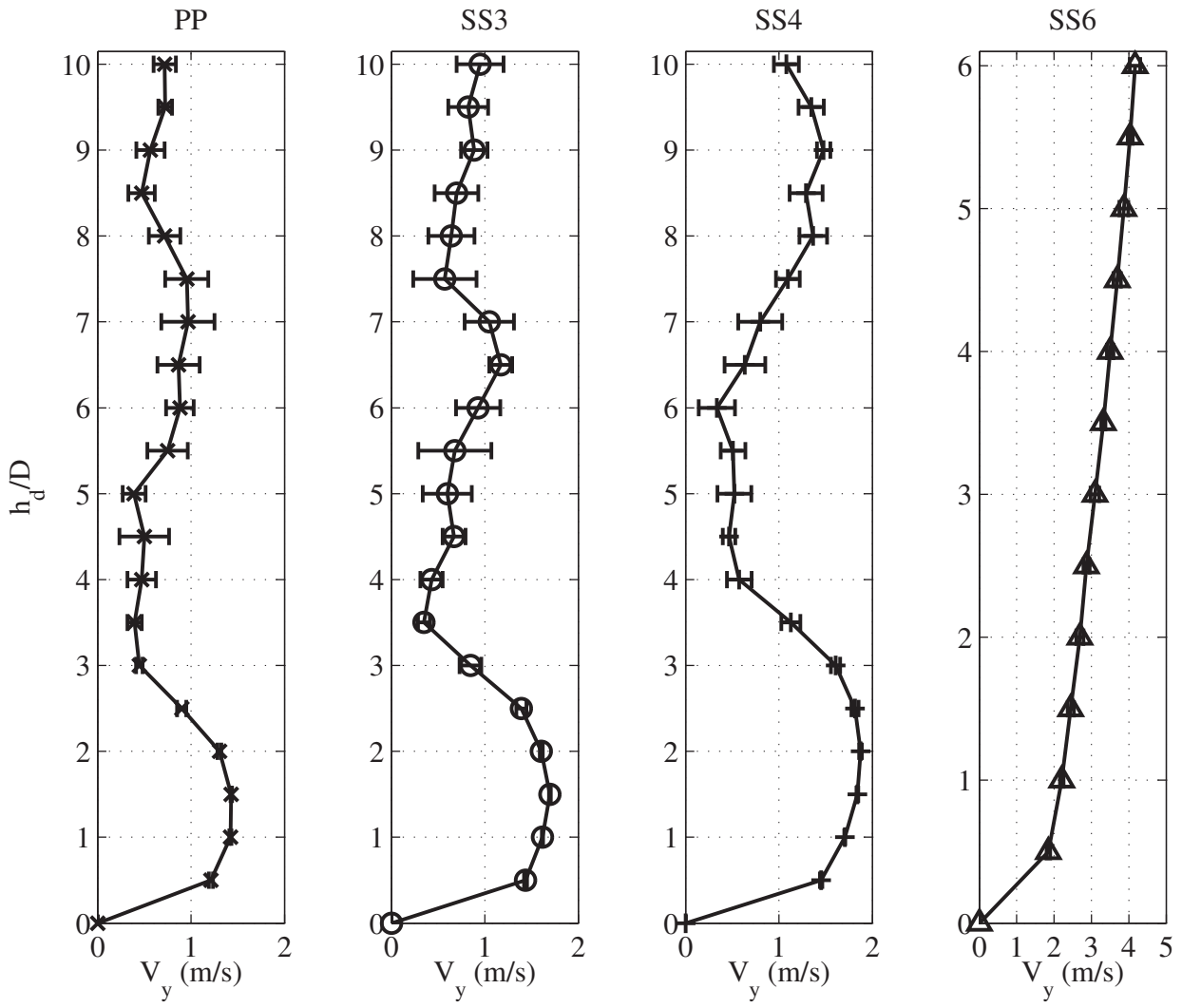

Figure 3.3: Velocity in the vertical direction at free surface exit versus release depth. The error bars are reported with a 95% confidence interval on the mean using a students-t distribution based on 10 runs from each depth for PP, SS3, SS4 and 2 runs for SS6.

after sufficient time and distance from rest underwater. Vortex shedding is directly coupled with decelerations demonstrating dependence of popup height on the point of free surface exit. Figures 3.3 and 3.4 illustrate the vertical velocity and acceleration, respectively, of a sphere at the free surface versus release depth. These figures are a composite of velocities and accelerations at the free surface for a given release depth. The error bars at any given depth are reported with a 95% confidence interval on the mean using a students-t distribution based on 10 runs for PP, SS3, SS4 and 2 runs for SS6. Vertical position data was extracted from images using a sphere tracker up until

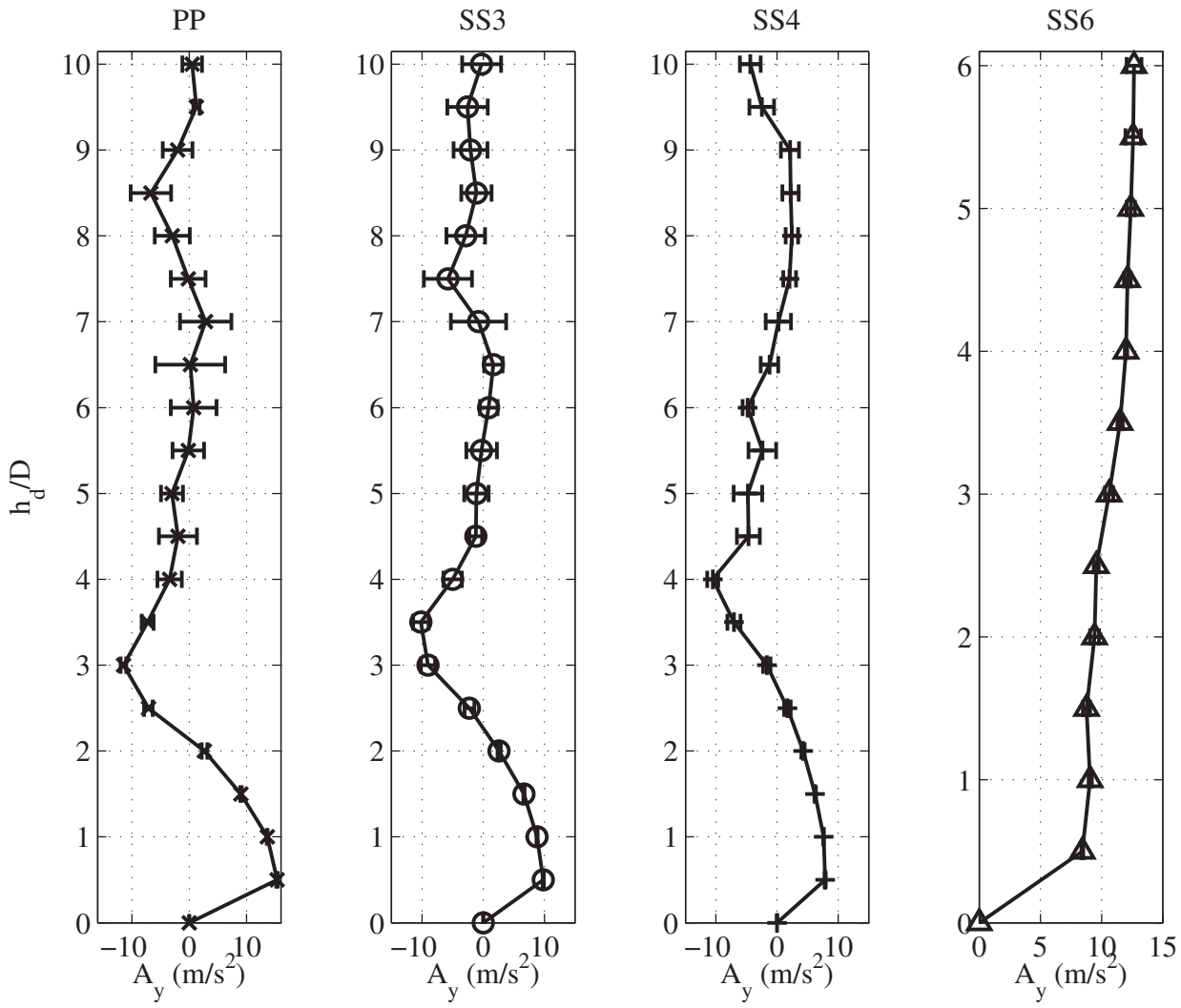

Figure 3.4: Acceleration in the vertical direction at free surface exit versus release depth. The error bars are reported with a 95% confidence interval on the mean using a students-t distribution based on 10 runs from each depth for PP, SS3, SS4 and 2 runs for SS6.

1/8th of the sphere remained visible below the free surface. After applying a quadratic fit to the position data, first and second derivates of the second order fit produced velocity and acceleration data, respectively, for the sphere at the free surface.

Shallow release depths show the greatest velocities and accelerations at the free surface corresponding with the largest popup heights. Increased release depths shows a decrease in velocity and accelerations, correlating with decreased popup heights. Decelerations correspond with lower popup heights and occur prior to the lowest heights. After reaching a minimum velocity,

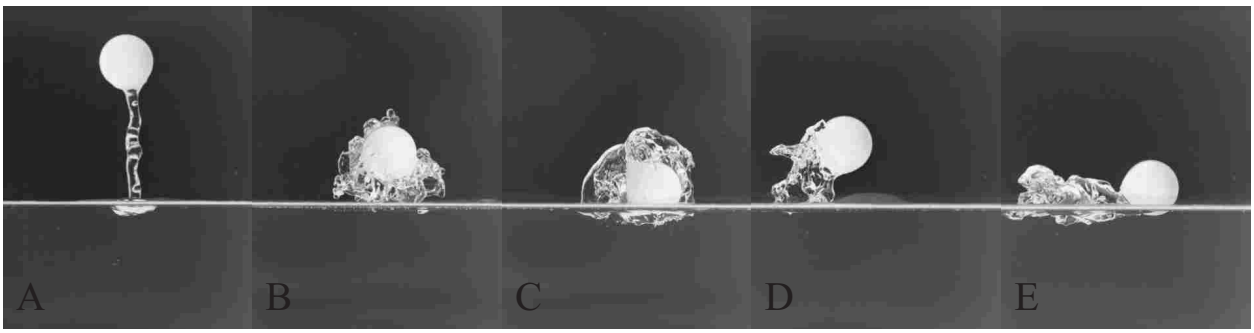

Figure 3.5: Still images of the apex of the popup trajectory of a pingpong ball corresponding to the popup data in Figure 3.2a. Released from depths: h_d/D = 1, 2.5, 4, 6.5, 9 resulting in popup heights of h_p/D = 3.3, 1.5, 0.92, 1.4, 1.0 for cases A, B, C, D, E respectively.

the velocity curve begins to oscillate similar to the oscillating popup heights seen in Figure 3.2a-c. Following the point of minimum popup height, decelerations are followed by accelerations corresponding to greater popup heights at the local maximum peaks. Velocities and accelerations will be used to further discuss regimes correlated with popup height, trajectories, and vortex shedding.

Still popup height images reveal that the popup event occurs differently for varying regimes as predicted by Bourrier [1]. Figure 3.2a-c shows a clear representation of the variation of regimes experienced as the free surface is breached based upon observation of the event and resulting popup height. Still images in Figure 3.5 represent the maximum popup height event for the pingpong ball at release depths h_d/D = 1, 2.5, 4, 6.5, 9 corresponding to A, B, C, D, E respectively in Figure 3.2a. The maximum popup height at A in Figure 3.5 depicts the sphere exiting the free surface during the accelerating regime. Figure 3.4 confirms the existence of the accelerating regime at h_d/D = 0.5 for the PP case with an acceleration of 15.3 m/s^2. Ascending buoyant spheres breaching and exiting the surface during the accelerating regime will experience a high exit velocity (1.2 m/s) resulting in a large popup height similar to the still image at A in Figure 3.5. Contributing to the ability of the sphere to reach such a high apex, along with high exit velocity and acceleration, is the trajectory of the sphere below the free surface which is completely vertical with no oscillations during ascension. The resulting popup trajectory above the water's surface is also completely vertical.

When ascending from the release depth, h_d/D = 2.5, which produces the popup height at image B in Figure 3.5, the sphere has moved from the accelerating regime into a transition regime

referred to as oblique. This claim is evident in the deceleration of -7.1 m/s^2 along with reduced popup height and velocity at free surface exit (0.9 m/s). Spheres ascending in the oblique regime experience a slight angle in the vertical trajectory without any oscillatory motion. The vertical path of the sphere above the free surface is similar to the path of the sphere in the accelerating case, the difference being the magnitude of the popup and also the noticeable amount of water pulled up with the sphere. The energy transferred from the rising sphere to the water during the popup event actually carries the fluid higher than the sphere. This phenomena is a result of wake and vortex formation and is present in the oblique and oscillatory regimes. Whereas the sphere in the accelerating regime pulls up a column of water with the sphere retaining the largest portion of the energy allowing greater popup heights.

Cases C and D in Figure 3.5 have exited the oblique regime and entered the oscillatory regime upon exiting the free surface. Trajectories during the oscillatory regime are vertical in the mean, with periodic oscillations. The still image at C in Figure 3.5 shows the lowest possible popup height, released from $h_d/D = 4$, where the sphere is said to 'kiss' the surface of the water. The surrounding water robs the energy of the sphere and only allows the sphere to reach the surface and skim across the surface, never actually leaping up out of the water. This event is caused by a shedding vortex just prior to free surface exit (illustrated in Section 3.4) around $h_d/D \approx 3$ where the largest deceleration (A_y = -11.5 m/s^2) occurs. This deceleration prior to exit produces a very low exit velocity (0.47 m/s) and popup height ($h_p/D = 0.92$). An ascending sphere that breaches the free surface during a curve or turn in the oscillatory path will result in a popup event similar to image C caused by a shedding vortex and large decelerations.

Image D reveals an entirely different popup result where the sphere creates separation and leaves the free surface. The sphere at D was released from a deeper release depth ($h_p/D = 6.5$) allowing the sphere to progress in the oscillating trajectory and exit the water at a point in the path after a vortex has been shed. Following the vortex shedding event, the sphere accelerates (A_y = 0.8 m/s^2) prior to free surface exit producing a vertical trajectory and greater exit velocity (0.87 m/s), and therefore, a greater popup height ($h_p/D = 0.92$). Case E in Figure 3.5 shows another popup only kissing the free surface. Similar to the progression of the oscillating path in case D and a deeper release depth ($h_d/D = 9$), a second vortex has had enough time and distance to form and shed prior to free surface exit. The result is another large deceleration prior to exit (A_y = -6.7 m/s^2)

along with a low exit velocity (0.57 m/s), non-vertical exit trajectory and low popup height (h_d/D = 1.0).

The behavior of the 6 inch stainless steel sphere (SS6) is much different compared to the other three spheres. Contrary to the oscillatory nature of the general curve of the popup data for the other three cases considered previously, the data of popup height versus release depth in Figure 3.2d show a linear trend. Beginning with the most shallow release depth, h_d/D = 0.5, the exit acceleration, velocity and resulting popup height reveals the smallest magnitudes: A_y = 8.4 m/s^2, V_y = 1.84 m/s and h_p/D = 2.1 respectively. The acceleration, exit velocity and popup height then increase with increasing release depth as seen in Figures 3.4, 3.3 and 3.2d. The maximum release depth is limited by the size of the glass tank being used for experimentation. The maximum release depth, h_d/D = 6, shows an acceleration of 12.7 m/s^2, exit velocity of 4.13 m/s producing a popup height of h_p/D = 8.42. The increasing acceleration, exit velocity and popup height demonstrates that the sphere remains in the accelerating regime for all release depths reported in the current study for the SS6 case.

The size of the glass tank limited release depth of the SS6 experiments which led to experimental procedures at a swimming pool. Attempts were made to collect data from deeper depths than the experimental tank allowed. The results of this data were skewed because of the lack of quiescence of the water in the swimming pool, and therefore are not presented here. Upon release, the sphere instantly began to oscillate vigorously during ascension, even at shallow release depths. This early onset of the oscillatory regime is due to the unsteady conditions of the water common to a swimming pool, adding to the importance of consistent experimental conditions through quiescent fluid. Buoyant spheres released in actual environments, where water is never quiescent, may demonstrate similar trends as in quiescent water. However, a high degree of repeatability cannot be expected under non-quiescent conditions. The current study is unable to draw conclusions about the maximum popup height of the SS6 case from experimentation. The trend of the popup height versus deeper release depths also remains unknown, i.e., whether or not the SS6 case data reaches a peak and then begins to oscillate with valleys and local maximum peaks similar to the data of the other three spheres presented previously.

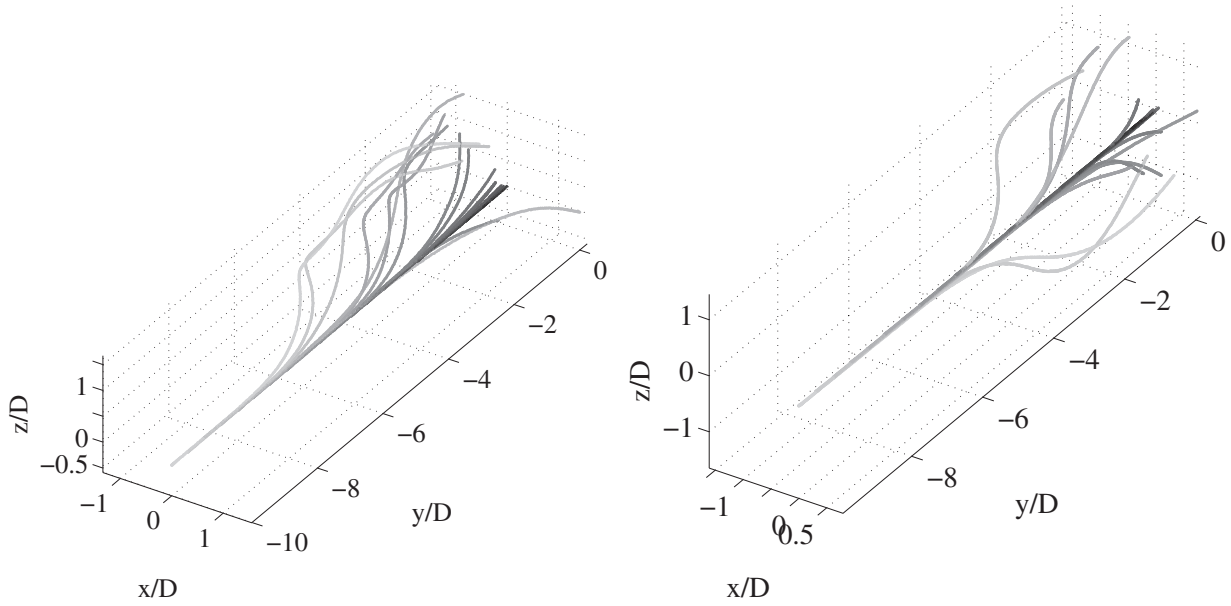

(a) ping pong (b) SS3

Figure 3.6: Isometric view of 3D trajectories of ascending spheres in water, ping pong ball (a) and SS3 (3 inch stainless steel) (b). There are 20 different trajectories for each sphere released from 20 release depths from 0.5 to 10 diameters below the free surface. Line shades represent different release depths: black = shallow, light = deep. Here, the y-axis is the vertical axis and each axis has been normalized by the respective sphere diameter.

3.3 Trajectories

Trajectories below the free surface have been the focus of much of the research performed in the past on rising buoyant spheres. Jenny et al. [12], Veldhuis et al. [13], and Horowitz et al. [8] based the prediction and definition of regimes experienced by rising buoyant spheres upon the nature of the path below the free surface. Trajectories for the spheres used in the current study will be presented here and correlated with regimes, exit acceleration and velocity, and resulting popup height data above the free surface discussed in section 3.2, similar to the work of Bourrier [1].

Depending on the release depth below the free surface, the regime experienced by the sphere upon exit of the free surface is altered. As previously discussed, the accelerating regime is seen early on in the spheres travel when released from rest, demonstrating accelerations and high velocities. After terminal velocity, a transition occurs when the sphere decelerates reducing velocity. The sphere briefly visits this transitional oblique regime before moving into the final

oscillatory regime where the sphere continues to decelerate until a vortex is shed after which the acceleration occurs until another vortex forms and sheds.The oscillatory path of the sphere in this final regime below the free surface, along with paths of the accelerating and oblique regimes, is visualized by the trajectories from varying release depths as shown in Figure 3.6 for the pingpong and SS3 spheres. The vertical axis is shown as y/D with the free surface set as zero and the release depth (h_d/D) increments in the negative y direction. For each sphere, full trajectories were extracted from experimental data using a direct linear transform (DLT) and shown from 20 release depths. Markers are plotted as black for shallow release depths and lighter shades for deeper release depths. The path of spheres in the accelerating and oblique regimes display very little deviation from the center line during ascension. As the release depth increases, the transition to a oscillatory regime is very obvious as the 3D trajectories leave the initial centerline and the oscillatory path sets in.

The onset of the vortex induced vibrations — the catalyst of transition to and existence of the oscillatory regime — appears earlier for spheres with a low mass ratio (m^*), as reported by Jenny et al. [12]. This claim is supported and confirmed by the isometric view of 3D trajectories in Figure 3.6. The mass ratio for the pingpong ball and SS3 sphere is 0.08 and 0.35, respectively. The trajectories of the ping pong ball in Figure 3.6a begin to deviate from the centerline much sooner from release than the SS3 case in Figure 3.6b. Focusing on the deepest release depth (light gray markers) from y/D = -10 (h_d/D = 10) for both spheres, the onset of vortex induced vibration begins to set in during ascension around y/D = -6 for the ping pong ball (Figure 3.6a), while the deviation for the SS3 case from the centerline is not noticeable until y/D = -4 (Figure 3.6b).

Once the sphere has transitioned into the oscillatory regime, the acceleration, velocity, and angle of trajectory at free surface exit varies greatly along with the resulting popup height, demonstrating dependence on release depth. While a sphere released from one particular release depth will result in consistent popup heights with very low error, observation of the popup event and popup data previously discussed in section 3.2 and displayed in Figure 3.2a-c give ample evidence of a variation of popup heights for a range of release depths for spheres in the oscillatory regime. Free surface exit angles along with complete trajectories within the oscillatory regime corresponding to the popup data in Figure 3.2a and the still images in Figure 3.5 are shown in Figure 3.7 for a ping pong ball at 3 different release depths (cases C,D,E). Release depths for cases

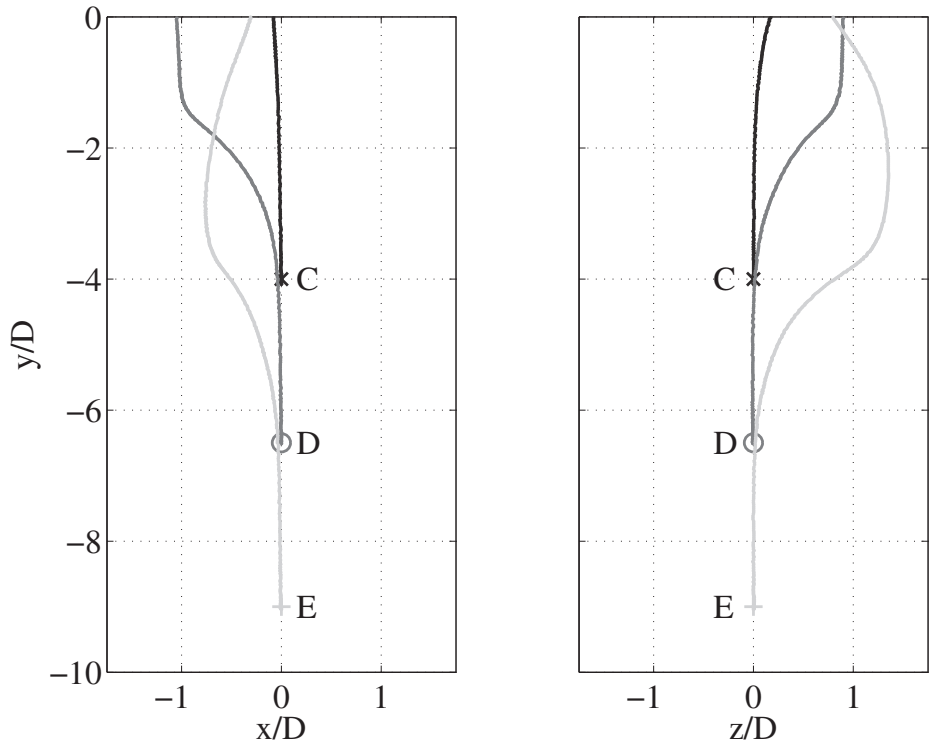

Figure 3.7: Trajectories of an ascending ping pong ball released from 3 different depths represented by different line shades, h_d/D = 4(darkest), 6.5, 9(lightest). Trajectories are shown in the x-y and z-y planes and correspond to the popup height data in Figure 3.2a and still images of the apex above the free surface in Figure 3.5. Cases C, D and E shown are released from depths which allow the sphere time and distance to enter the oscillatory regime before free surface exit.

C, D, and E are h_d/D = 4, 6.5, 9, with acceleration and velocity at exit, A_y = -3.4, 0.2, -2.0 m/s^2 and V_y = 0.47, 0.87, 0.57 m/s, respectively, producing a popup height of h_p/D = 0.92, 1.4, 1.0 respectively. The trajectories are displayed in two planes, x-y and z-y, with the y axis being the vertical axis and each axis normalized by diameter D. Cases C, D and E shown are released from depths which allow the sphere time and distance to enter the oscillatory regime prior to free surface exit.

Focusing on case C in Figures 3.2a, 3.5, and 3.7, the sphere has entered the oscillatory regime prior to reaching the free surface and the angle of trajectory at free surface exit has deviated from vertical because of a vortex being shed. This non-vertical angle, deceleration (A_y = -3.4 m/s^2) and low exit velocity (V_y = 0.47 m/s) causes the sphere to only kiss the surface with no separation from the water, resulting in the lowest popup height for the ping pong ball (h_p/D = 0.92). The

trajectory for case E was released from a much deeper release depth (h_d/D = 9) and allowed the sphere to move through a period in the oscillatory path, allowing time for a second vortex to form and shed, such that the exit angle, deceleration (A_y = -2.0 m/s^2) and velocity (V_y = 0.57 m/s) at the free surface is very similar to that of case C. The still image popup event for case E is likewise similar to case C (see Figure 3.5) as is the magnitude of the popup height, h_p/D = 1.0.

The oscillating trajectory for case D in Figure 3.7 (h_d/D = 6.5) verifies that the sphere has entered into the oscillatory regime well before interaction with the free surface, similar to cases C and E. The difference for case D is the point at which the sphere breaches the free surface during the oscillatory path being in between vortex shedding events, demonstrating release depth as the determining factor for the type of exit angle, acceleration and velocity realized at the free surface. As seen in Figure 3.7, the angle of trajectory at the top of the frame is completely vertical in both planes for case D. This vertical angle coupled with acceleration (A_y = 0.2 m/s^2) and high velocity (V_y = 0.87 m/s) at free surface exit allow the sphere to pop up above the water and create noticeable separation resulting in a greater popup height (h_p/D = 1.4) compared to cases C and E, which also exit the free surface in the oscillatory regime.

In order to better visualize the deviation from the initial vertical trajectory as the sphere moves into the oscillatory regime, a radial deviation from the central y-axis was calculated. The radial center is the vertical y-axis with (x, z) = (0,0) as the origin. Radial deviation R is the absolute magnitude from the central y-axis (radial center) and is calculated as follows

$$R = \sqrt{x^2 + z^2} \tag{3.1}$$

where x and z are the distance from the origin along the x and z axes respectively.

Figure 3.8 depicts the underwater trajectory as radial deviation R from the central y-axis of an ascending sphere released from a shallow release depth which results in the maximum popup height above the free surface for 3 spheres: pingpong, SS3, and SS4. Release depth for each case is specified by the marker **o** with depths: h_d/D = 0.5, 1, 1.5, for pingpong, SS3, and SS4 respectively. The maximum popup height achieved for the three cases are h_p/D = 3.29, 2.25, 2.17, respectively as seen in Figure 3.2a-c with accelerations and velocities at exit of A_y = 15.3, 8.8, 6.2 m/s^2 and V_y = 1.2, 1.67, 1.84 m/s, respectively. The vertical nature of the trajectory confirms each sphere is in the

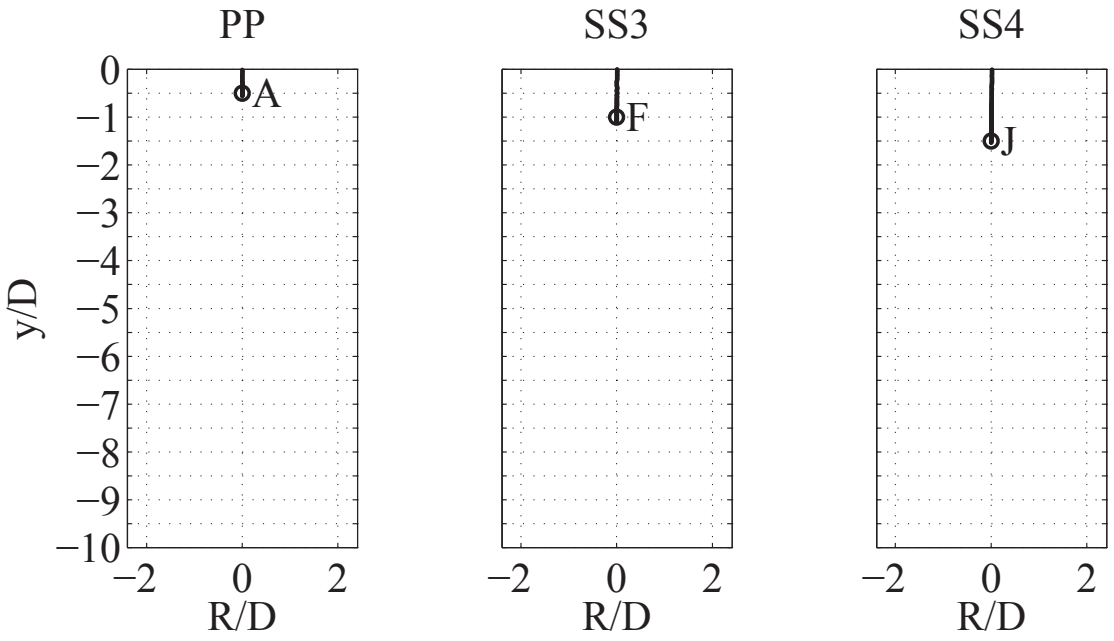

Figure 3.8: Trajectory plotted as radial deviation R from the central y axis of a sphere released from release depth specified by the marker **o**: h_d/D = 0.5, 1, 1.5, for PP, SS3, SS4 respectively. The trajectories correspond to the maximum popup height for the three cases: h_p/D = 3.29, 2.25, 2.17, respectively as seen in Figure 3.2a-c. The vertical nature of the trajectory reveals that the sphere remains in the accelerating regime for each case.

accelerating regime based on trajectory. The large acceleration at free surface exit gives evidence that each sphere is in fact in the accelerating regime, giving explication to maximum popup heights from these release depths. The trajectory for the ping pong ball corresponds to case A discussed previously in Figures 3.2a and 3.5.

Figure 3.9 shows the underwater trajectory plotted as radial deviation R from the central y-axis of an ascending sphere released from deeper release depths, h_d/D = 4, 5, 6, for pingpong, SS3, SS4 respectively. The trajectories here reveal that the sphere has transitioned from the accelerating regime and into the beginning stages of the oscillatory regime upon exiting the free surface. The path of the sphere shows an angled trajectory at the free surface as a result of deceleration (A_y = -3.4, -1.1, -4.8 m/s^2) and low velocity (V_y = 0.47, 0.60, 0.33 m/s) at breach and exit, resulting in a very low popup height: h_p/D = 0.92, 0.97, 0.70, respectively. Spheres released from these depths show the lowest popup heights as seen in Figure 3.2a-c. This deceleration due to a vortex shedding event is the contributing factor to the inability of the sphere to separate from the free

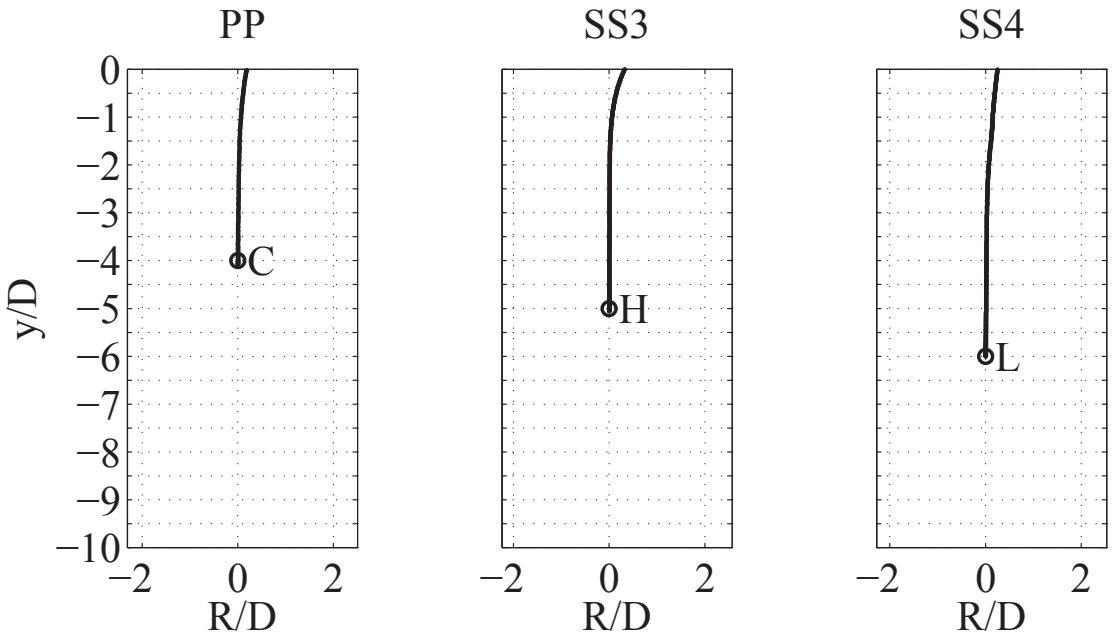

Figure 3.9: Trajectory plotted as radial deviation R from the central y axis of a sphere released from the release depth specified by the marker **o**: h_d/D = 4, 5, 6, for PP, SS3, SS4 respectively. The trajectories correspond to the minimum popup height for the three cases: h_p/D = 0.92, 0.97, 0.70, respectively as seen in Figure 3.2a-c. The trajectory reveals a deviation from the centerline axis and shows that the sphere has transitioned into the beginning stages of the oscillatory regime, exiting the free surface at an angle.

surface causing it to skim along the surface, or kiss the surface as seen in Figure 3.5 case C. The trajectory for the pingpong ball corresponds to case C discussed previously in Figures 3.2a and 3.5. The radial shift trajectory confirms the previous results and discussion that the sphere transitions from a vertical trajectory in the accelerating regime to a oscillatory regime at free surface exit.

Increasing the release depth results in trajectories plotted as radial deviation R from the central y-axis in Figure 3.10, with release depths at h_d/D = 6.5, 6.5, 9, for pingpong, SS3, SS4 respectively. The paths here confirm that spheres released from these depths are well into the oscillatory regime as seen by the radial deviation. The gap in the plotted trajectory for the SS4 case is from the bottom of the sphere being below the bottom of the frame of raw images when tracking the sphere. The path is completely vertical from the release point to where the plotted trajectory appears. The sphere reaches the free surface at a point in the oscillatory path which allows a vertical exit angle, well after the vortex shedding event. The sphere is now accelerating (A_y = 0.2,

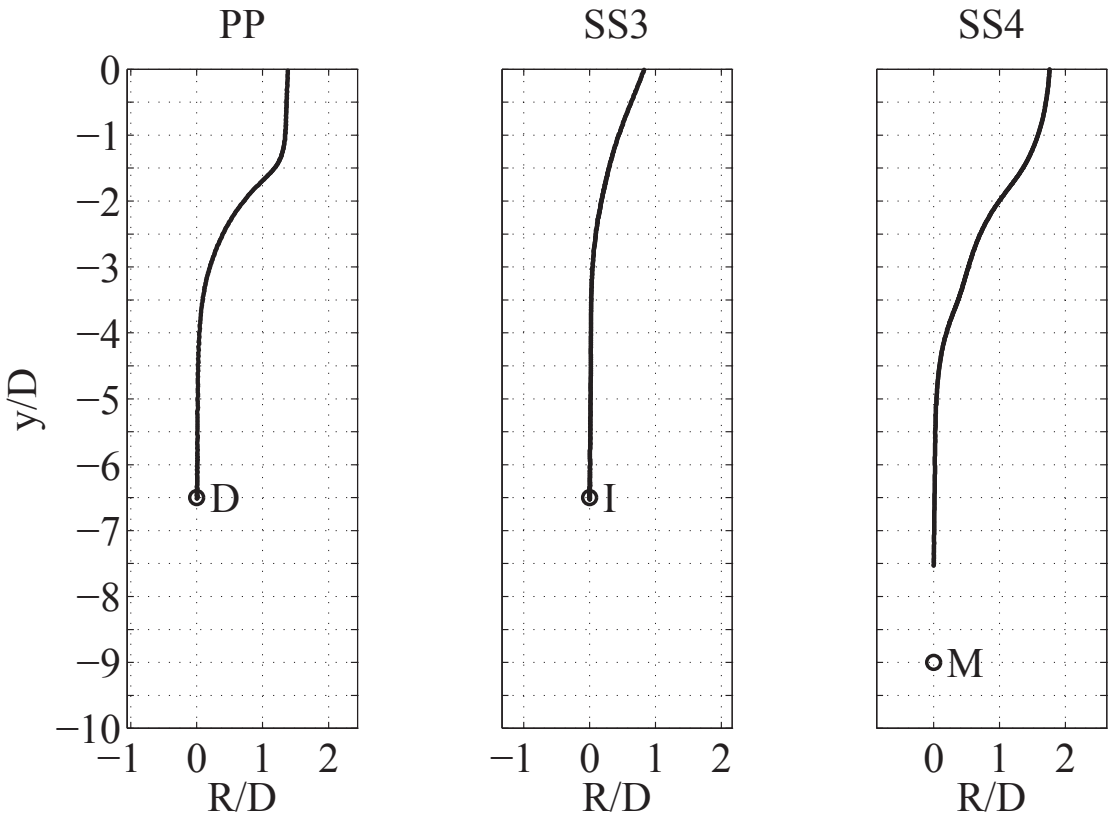

Figure 3.10: Trajectory plotted as radial deviation R from the central y axis of a sphere released from the release depth specified by the marker **o**: h_d/D = 6.5, 6.5, 9, for PP, SS3, SS4 respectively. The trajectories correspond to a local maximum popup height for the three cases: h_p/D = 1.42, 1.27, 1.61 , respectively, as seen in Figure 3.2a-c. The trajectory reveals a deviation from the centerline axis and shows the sphere is well into the oscillatory regime for each case, exiting the free surface with a vertical path and allowing the sphere to separate from the surface of the water.

1.7, 2.1 m/s^2) which results in high exit velocities (V_y = 0.87, 1.2, 1.5 m/s). The magnitude of the popup heights are larger than those resulting from the release depths shown in Figure 3.9, but not as great as the maximum popup heights achieved in Figure 3.8. These popup heights are at a local maximum peak in the experimental popup data presented in Figure 3.2a-c, h_p/D = 1.42, 1.27, 1.61 respectively. The far left trajectory of the ping pong ball corresponds to case D discussed previously in Figures 3.2a and 3.5.

In previous discussions and during experimentation, the free surface has been the stationary origin with rising spheres approaching, breaching and exiting the free surface. The release depth has been the altered variable as a normalized distance below the free surface. Changing the point of

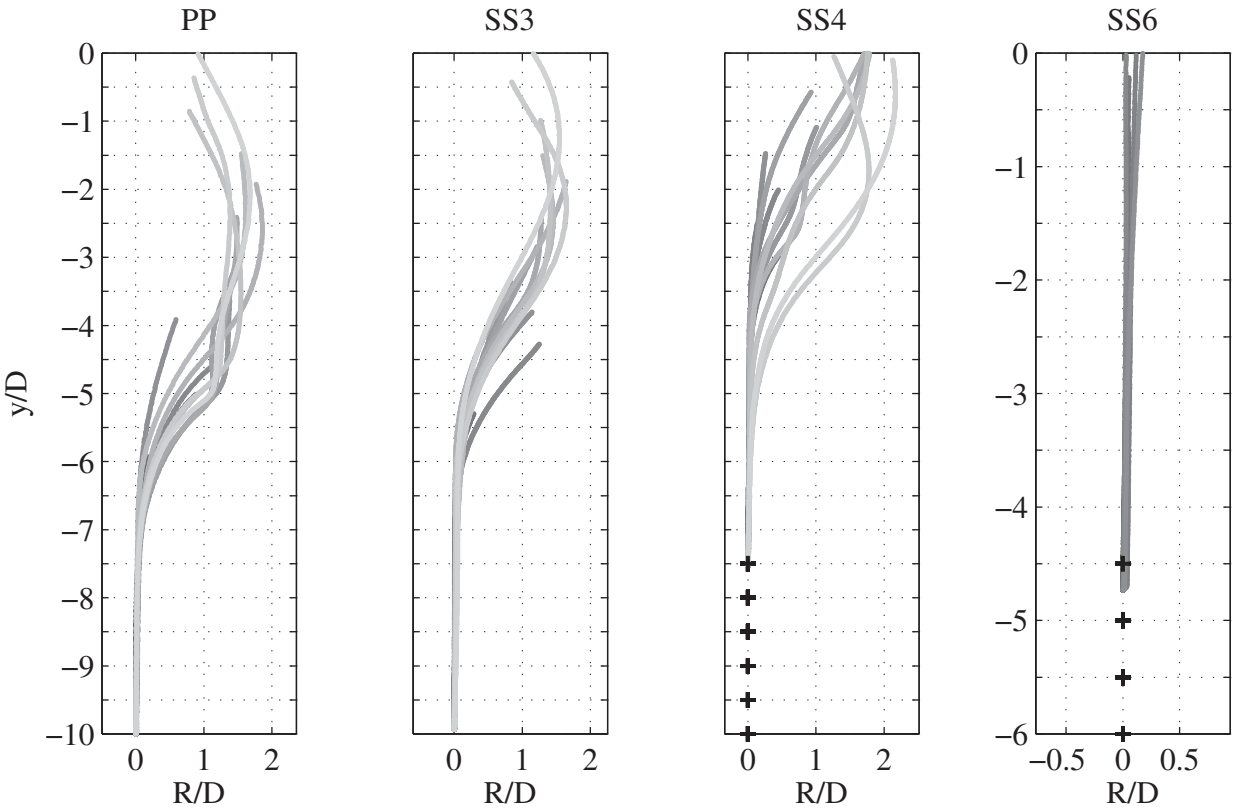

Figure 3.11: Trajectories plotted as radial deviation R from the vertical central y-axis for spheres from left to right: ping pong, SS3, SS4, SS6. Each release depth has been normalized to the origin. The radial shift R and the vertical y-axis have been normalized by the respective diameter D.

release to now be the stationary origin and normalizing the point of release depth to this new origin of the central y-axis allows the point of release to be viewed as the stationary variable, and the free surface can then be visualized as a moving variable. Following this new frame of reference, plotted trajectories as radial deviation from the vertical central y-axis as seen in Figure 3.11 reveal the paths from each release depth lining up with very little variation as the free surface increases distance from the release point at y/D = -10, in essence increasing the release depth. Trajectories in Figure 3.11 are plotted for each sphere used in the current study: ping pong, SS3, SS4 and SS6. The radial shift R and the vertical y-axis are normalized by respective diameter D. The two plots on the right for the SS4 and SS6 cases show a void of data below y/D = -7.5 and -4.5 respectively. This lack of data is due to the release depths falling below the bottom of the camera frame during

experimental runs and processing. The markers show where the release depths occurred within the gap of data.

Through observation of the rectilinear trajectories of the SS6 case of Figure 3.11, the deepest release depths appear to reach the initial stages of the transition or oblique regime, based on definitions of past research. However, the experimental data show increasing acceleration (Figure 3.4) and popup heights (Figure 3.2d) with increased release depth revealing that the SS6 case remains in the accelerating regime for the depths in this study. Based on the small radial deviation from the central y-axis, it is possible to hypothesize that the SS6 case is in the beginning stages of the oblique regime and it would follow that the curve of the popup height data in Figure 3.2d would begin to plateau instead of following a continual linear increase with release depth.

3.4 Vortex Shedding

Past research has shown the role which wake formation and vortex shedding play in the oscillatory path of a rising buoyant sphere. Veldhuis et al. [13] give a thorough description of wake formation and structures of a sphere held fixed in a uniform flow, where the wake is symmetric at low *Re* and transitions to irregular and finally turbulent as *Re* increases. Horowitz et al. [17] performed visualization experiments and PIV measurements of the vortical structures left in the wake of a rising sphere. Visualization was performed on freely rising spheres and PIV was performed on a tethered sphere in a computer controlled tow tank. These studies resulted in the discovery of patterns and wake modes unlike any found previously for either fixed or vibrating spheres. In the present study, PIV velocity measurements and vorticity calculations have been performed on the wake formation, separation and detaching vortical structures of freely rising spheres approaching the free surface. As previously noted, values of *Re* for the current study is significantly higher ($1\times10^4 < Re < 6\times10^5$) than *Re* in experiments reported by Veldhuis ($Re \approx 345$) and Horowitz ($Re \approx 450$).

Regimes experienced by an ascending buoyant sphere have been defined through accelerations, velocities, trajectory, and popup height. This section continues the discussion of regimes through presenting results of 2D PIV of rising spheres near the free surface. Raw images were captured at 1000 fps of spheres rising in a fluid with polyamide seeding particles illuminated by a laser sheet from a class 4, 527 nm, YLF Quantronix Darwin-Duo laser. PIV experiments were per-

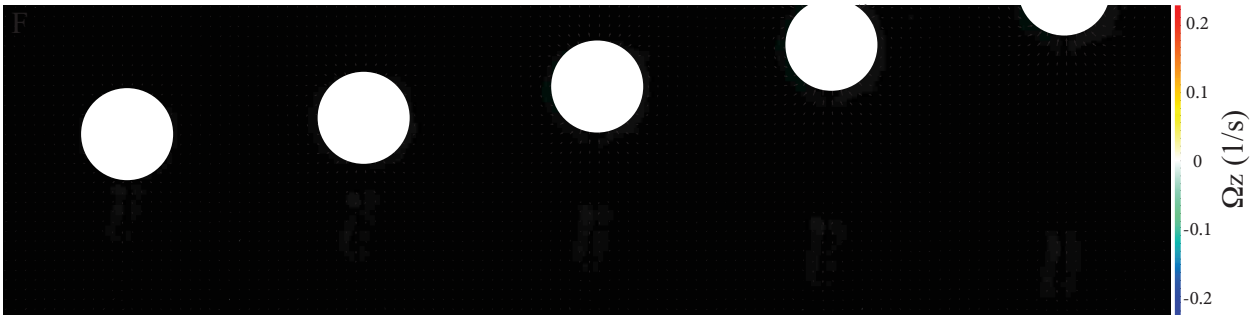

(a) SS3 $h_d/D = 1$

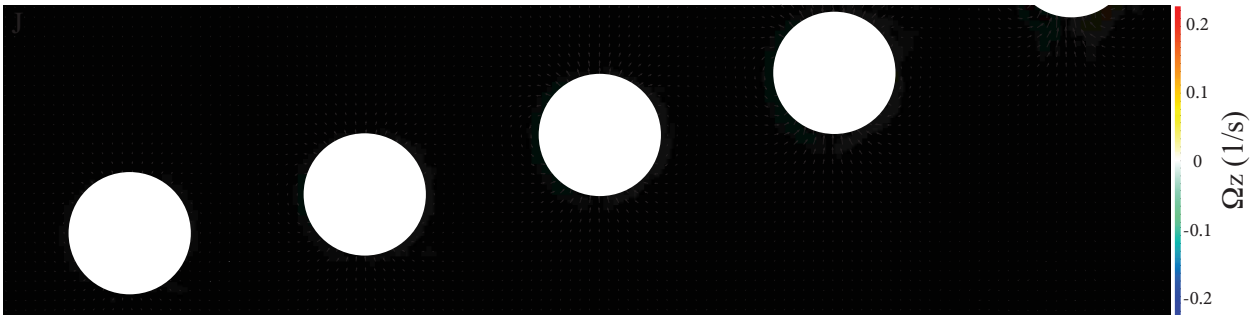

(b) SS4 $h_d/D = 1.5$

Figure 3.12: PIV vector fields and vorticity shown as color contours of a time series sequence of rising sphere released from shallow release depths: $h_d/D = 1$(a), 1.5(b). Release depths for cases F and J correspond to spheres rising in the accelerating regime resulting in the highest popup heights ($h_p/D = 2.25$, 2.17) as seen in Figure 3.2b-c. The sphere is released from rest within the bottom of the frame (far left) and rises towards the free surface (top of frame). The time step in between frames for each time series is $dt = 20$(a), and 24 ms(b). $Re = 1.1\times10^5$(a) and 1.7×10^5(b))

formed following the same release methods and experimental process outlined for the popup data. Post-processing was performed using a LaVision software package. Vector fields are presented with vectors showing velocity magnitude and vorticity (Ω_z) shown as the vector background color.

Figure 3.12 shows PIV results for SS3 and SS4 spheres, released from depths $h_d/D = 1$, and 1.5 respectively. The two cases shown in Figure 3.12 are released from rest within the far left frame and reach the free surface (top of frame) while in the accelerating regime. Here, wake and vortex formation is still in the early stages of development and has not created separation from the sphere when free surface exit occurs. A completely vertical trajectory is allowed due to the absence of forces from vortex interaction. Given these conditions the sphere experiences very little resistance while accelerating from rest to free surface exit, resulting in the greatest popup heights ($h_p/D = 2.25$, 2.17). Cases F and J correspond to the popup height data in Figure 3.2b-c and the

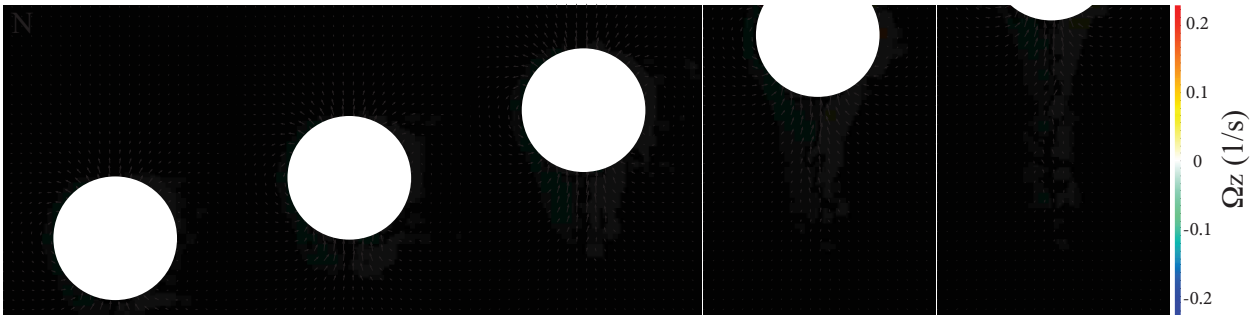

(a) SS6 $h_d/D = 3$

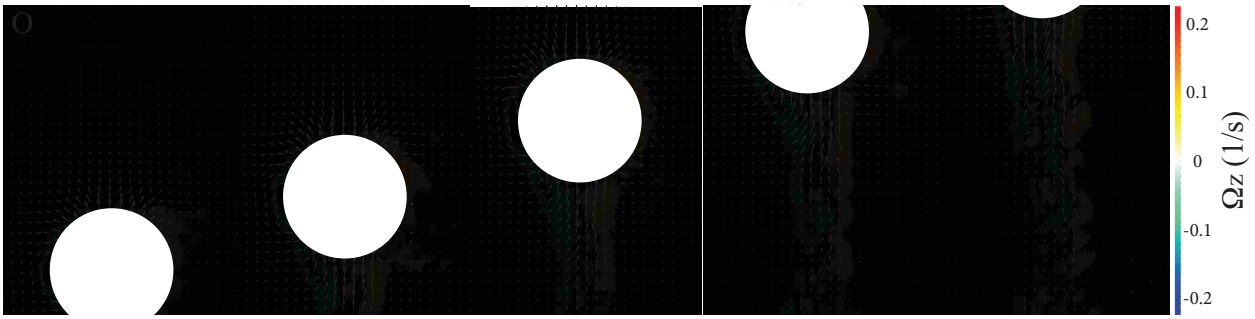

(b) SS6 $h_d/D = 6$

Figure 3.13: PIV vector fields and vorticity shown as color contours of a time series sequence of rising sphere released from: $h_d/D = 3$(a) and 6(b). Release depths for cases O and P correspond to the popup heights ($h_p/D = 4.79$, 8.42) as seen in figure 3.2d. The sphere is released from rest and rises towards the free surface (top of frame). The time step in between images for each time series is dt = 17(a), and 13 ms(b). $Re = 4.2\times10^5$(a) and 5.6×10^5(b).

trajectory data in Figure 3.8. The yellow-green structure behind the sphere in Figure 3.12a is the suction cup falling after release. While the wake dynamics of the accelerating regime may seem trivial, PIV visualization of the physics of wake formation and separation confirms that vortex formation is minimal.

Two more cases are shown in figure 3.13 of a SS6 sphere approaching and exiting the free surface (top of frame) within the accelerating regime. Release depths for these two cases are h_d/D = 3 and 6 resulting in popup heights of h_p/D = 4.79, and 8.42 respectively (cases O and P in figure 3.2d). Although wake formation for these two cases is much more developed than those previously discussed in figure 3.12, the popup height is significantly higher. The *Re* of the spheres at free surface exit from these release depths are much greater ($Re = 4.2\times10^6$(a) and 5.6×10^6(b)) than the cases shown in figure 3.12 ($Re = 1.1\times10^5$(a) and 1.7×10^5(b)). The larger diameter and

velocities of the SS6 cases transition the sphere into the turbulent regime, reducing significantly the coefficient of drag ($C_d(Re)$) and allowing the wake to separate much farther back on the sphere (120°) when compared to spheres within the laminar regime (82°). The change in angle at which wake separation occurs for a turbulent case significantly reduces the forces from vortex formation on a rising sphere, allowing the sphere to exit the free surface at a much greater velocity resulting in more dramatic popup heights.

The wake structure behind the sphere in figure 3.13a is uniform and symmetric, justifying a completely vertical trajectory during ascension in the accelerating regime. The wake of the sphere in figure 3.13b displays asymmetry with a vortex forming on the left side of the sphere. This small vortex contributes to a slightly oblique angle in the vertical trajectory as seen previously in figure 3.11(far right), suggesting evidence that a hypothesis of the SS6 sphere beginning to transition from the accelerating regime into the oblique regime may be correct. While the trajectory gives evidence of the oblique regime, as defined by trajectories and popup data for spheres of lower *Re*(laminar), the sphere is still accelerating at exit with increasing popup height, confirming the acceleration regime at exit. For spheres rising in the laminar regime, an oblique vertical trajectory reduces the popup height. In contrast, the experimental data of accelerations and popup height for case O show that an oblique trajectory does not signify a reduced popup height. More experimental research of spheres rising within the turbulent regime must occur in order to draw conclusions and explain this discrepancy.

Figure 3.14 shows vector fields and vorticity as color contours for the SS3 sphere released from depth h_d/D = 2.5. Release depth for case G corresponds to spheres exiting the free surface during the oblique regime resulting in a popup height (h_p/D = 1.51) as seen in figure 3.2b. The sphere is released from rest and enters the bottom of the frame (far left) and rises towards the free surface (top of frame). When compared to the wake of spheres in the accelerating regime (figure 3.12), there is evidence that the wake development is more advanced with vortex structures forming before the free surface. Vortical structures not yet detached from the back of the sphere contribute to the slight oblique angle in the vertical trajectory along with a deceleration (A_y = -2.2 m/s^2), lower exit velocity (V_y = 1.4 m/s) and consequentially lower popup height when compared to the accelerating regime.

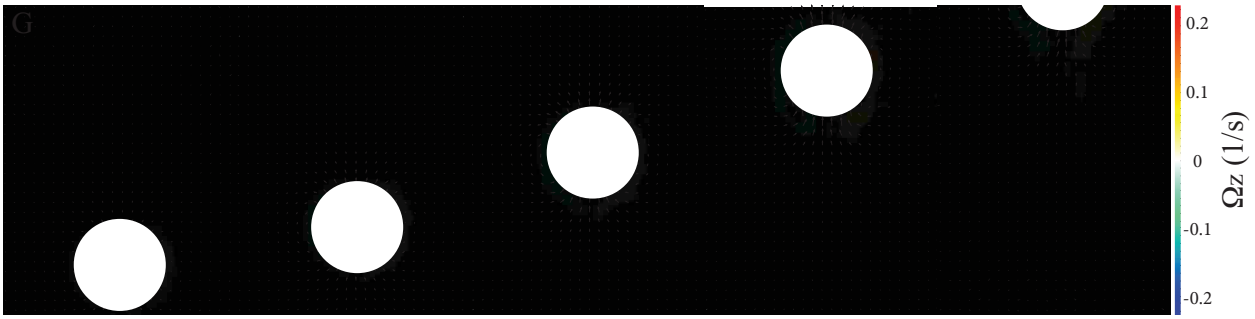

(a) SS3 $h_d/D = 2.5$

Figure 3.14: PIV vector fields and vorticity shown as color contours of a time series sequence of a SS3 sphere rising from release depth: $h_d/D = 2.5$. Release depth for case G corresponds to spheres exiting the free surface during the oblique regime resulting in a popup height ($h_p/D = 1.51$) as seen in figure 3.2b. The sphere is released from rest and rises towards the free surface (top of frame). The time step in between frames for each time series is dt = 30. $Re = 9.5\times10^4$.

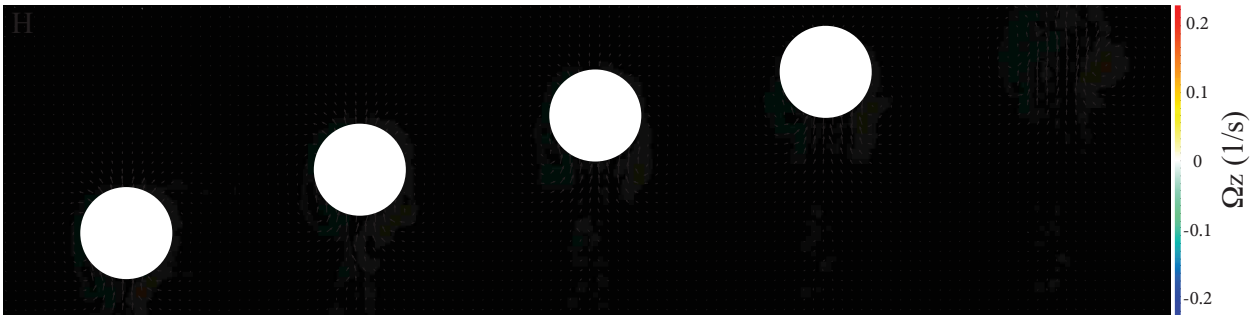

(a) SS3 $h_d/D = 5$

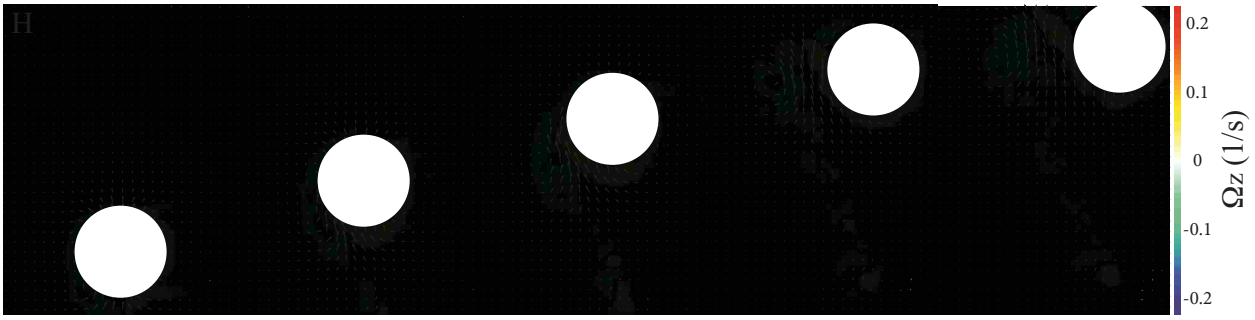

(b) SS3 $h_d/D = 5$

Figure 3.15: PIV vector fields and vorticity shown as color contours of a time series sequence of rising spheres of equal diameter released from the same release depth: $h_d/D = 5$. Release depths for case H correspond to spheres exiting the free surface during the oscillatory regime with trajectories displayed in figure 3.9 resulting in popup heights ($h_p/D = 1.51, 1.88$) as seen in figure 3.2b. The vortex has formed near the back of the sphere and is in the process of shedding as the sphere approaches the free surface (top of the frame). The time step in between frames for each time series is dt = 24. $Re = 4.1\times10^4$.

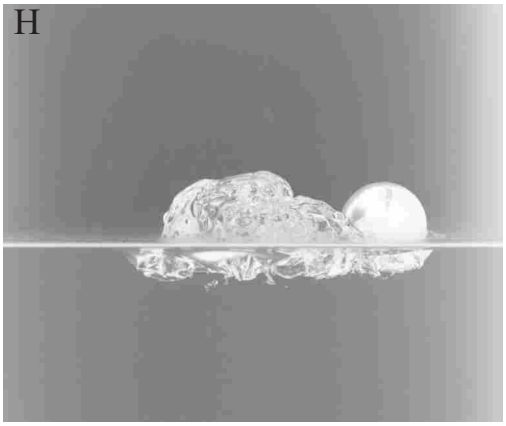

Figure 3.16: Still image of popup event at apex of a SS3 sphere released from h_p/D = 5. The plume left of the sphere is caused by vortex shed prior to free surface breach as seen in the PIV images in figure 3.15b.

PIV vector fields and vorticity shown as color contours of spheres rising and exiting the free surface during a vortex shedding event in the oscillatory regime are shown in figure 3.15. Both sequences display two independent releases of the same sphere (SS3) released from the same release depth (h_d/D = 5). PIV data for case H correspond with trajectories displayed in figure 3.9 resulting in popup height, h_p/D = 0.97, as seen in figure 3.2b. The sphere is released from rest, enters the bottom of the frame (far left) and rises towards the free surface (top of frame).

The vector fields in figure 3.15a show vortex formation and shedding which cause the sphere to leave the plane of the laser (into the page) at the far right image. The sphere experiences a large deceleration (A_y = -5.0 m/s^2) prior to the shedding event in the center image, and continued deceleration (A_y = -5.0 m/s^2) at free surface exit after the shedding of the vortex in between the last two frames. The deceleration of the sphere is caused by forces from the growing vortex in the wake of the sphere. The vortices on both sides of the sphere spread outward during ascension until shedding occurs. This causes the sphere to pitch out of the surface at an angle with a reduced speed, effectively reducing the popup magnitude.

The images in figure 3.15b reveal vector fields of a separate release of the same sphere released from the same depth. Although the sphere jogs to the right after the shedding event in the fourth frame, it remains in the plane of the laser capturing the vortex being shed. As the sphere enters the frame (far left), vortical structures are present. The vortex forming on the left side of

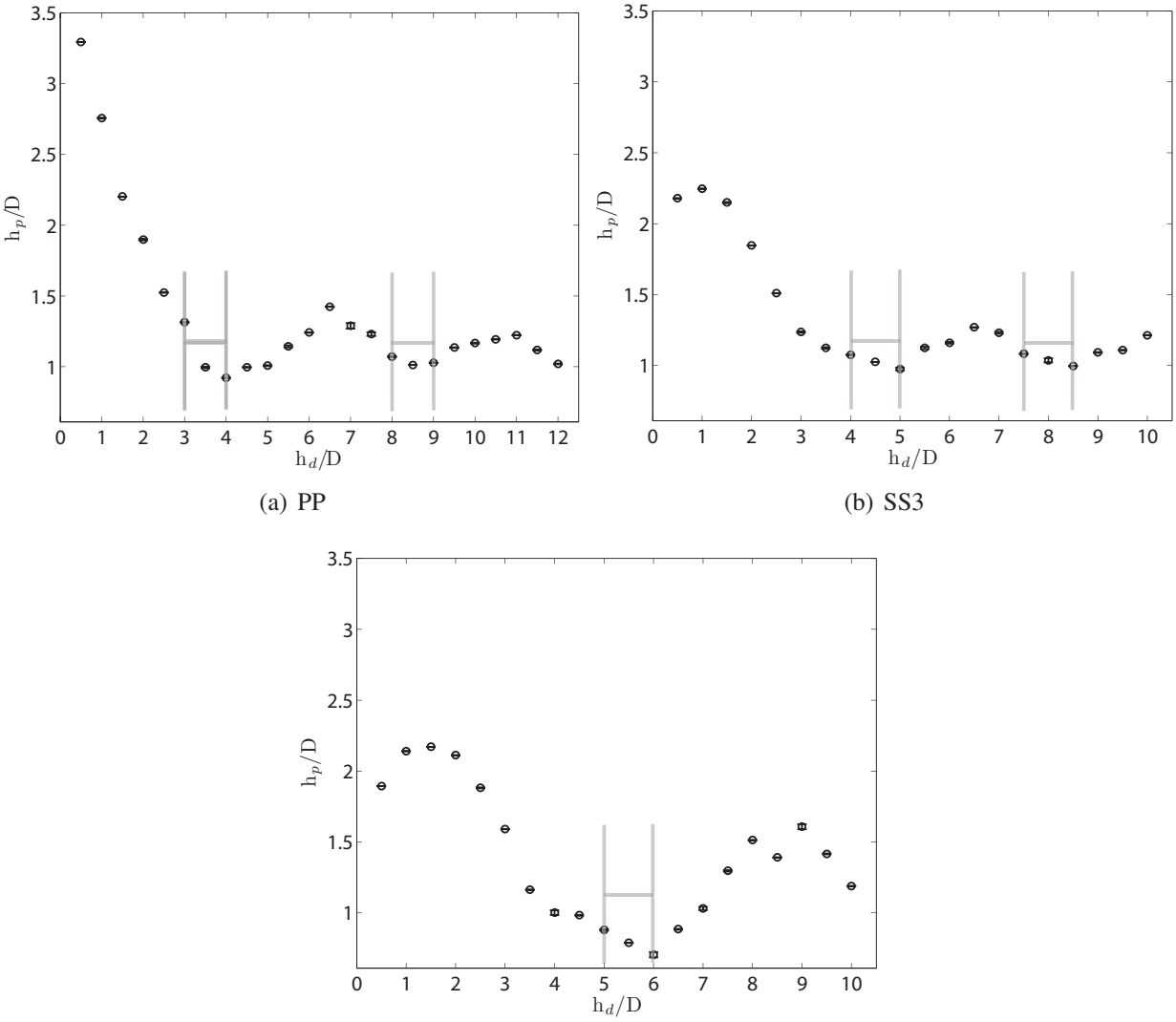

(a) PP

(b) SS3

(c) SS4

Figure 3.17: Vortex shedding event at specified h_d/D ($\pm$ 0.5D).

the sphere is noticeably larger than the right vortex and increases dramatically in size with each time step. Shedding of the vortex occurs somewhere in between the left-center and center frames (images 2 & 3 from left) creating a jet flowing past the left of the sphere seen in the center image. This shedding event causes the sphere to decelerate and deviate from a vertical trajectory, jogging off to the right just prior to breaching the free surface, causing the sphere to pitch out of the surface (kiss the surface) at an angle with reduced velocity and popup magnitude. The simultaneous event

of the jet, caused by the shedding vortex, and sphere exiting the free surface is captured beautifully with a high speed camera shown in figure 3.16.

Figure 3.17 shows the depths where a vortex shedding event occurs. The location of the depth is shown with a tolerance of $\pm$ 0.5D.

3.5 *Re* at Free Surface Exit

The non-dimensional number *Re* compares effects of momentum to the effects of viscosity ($Re = \rho_f VD/\mu$). Relating popup height to *Re* number adds to the discussion of the underlying fluid dynamics of rising spheres at the free surface through the viewing glass of momentous (diameter and velocity) and viscous (μ, wake separation, vortex shedding) effects of the flow. *Re* was calculated using the velocity extracted from the popup data as explained in Section 3.2. Figure 3.18 shows the *Re* vs popup height for all spheres and release depths in the current study extracted from experimental data. The data is displayed on a semi-logarithmic plot with the x-axis shown on a logarithmic scale. The dotted line shows the predicted popup height versus *Re* for each sphere and release depth performed in the experimental study.

Spheres released from shallow release depths show momentous effects dominating the flow, resulting in higher *Re* and popup heights as seen in cases A, F, and J (figure 3.2a-c). These cases, highlighted in rectangles, discussed throughout this paper have been classified as spheres rising in the accelerating regime during free surface exit resulting in the highest possible *Re* and popup height for the respective sphere diameters (pingpong, SS3, and SS4).

Viscous effects are more present with increased release depth, demonstrated as lower *Re* and h_p/D as seen in cases B, G, and K. These cases show release depths $h_d/D = 2.5$ for pingpong, SS3, and SS4 spheres and have been classified in the oblique regime. Any other depths show either equal or lesser *Re* and h_p/D values, showing dominant viscous effects for cases at deeper release depths due to wake separation and vortex shedding.

The data trend shows increasing *Re* for larger sphere diameter as expected, with the SS6 case transition from laminar to the turbulent regime. The viscous forces due to pressure drag are significantly lower for the SS6 case within the turbulent regime where wake separation occurs farther behind the sphere ($\approx$120°). This reduction in pressure drag allows for much greater popup heights in general when compared to spheres rising in the laminar regime.

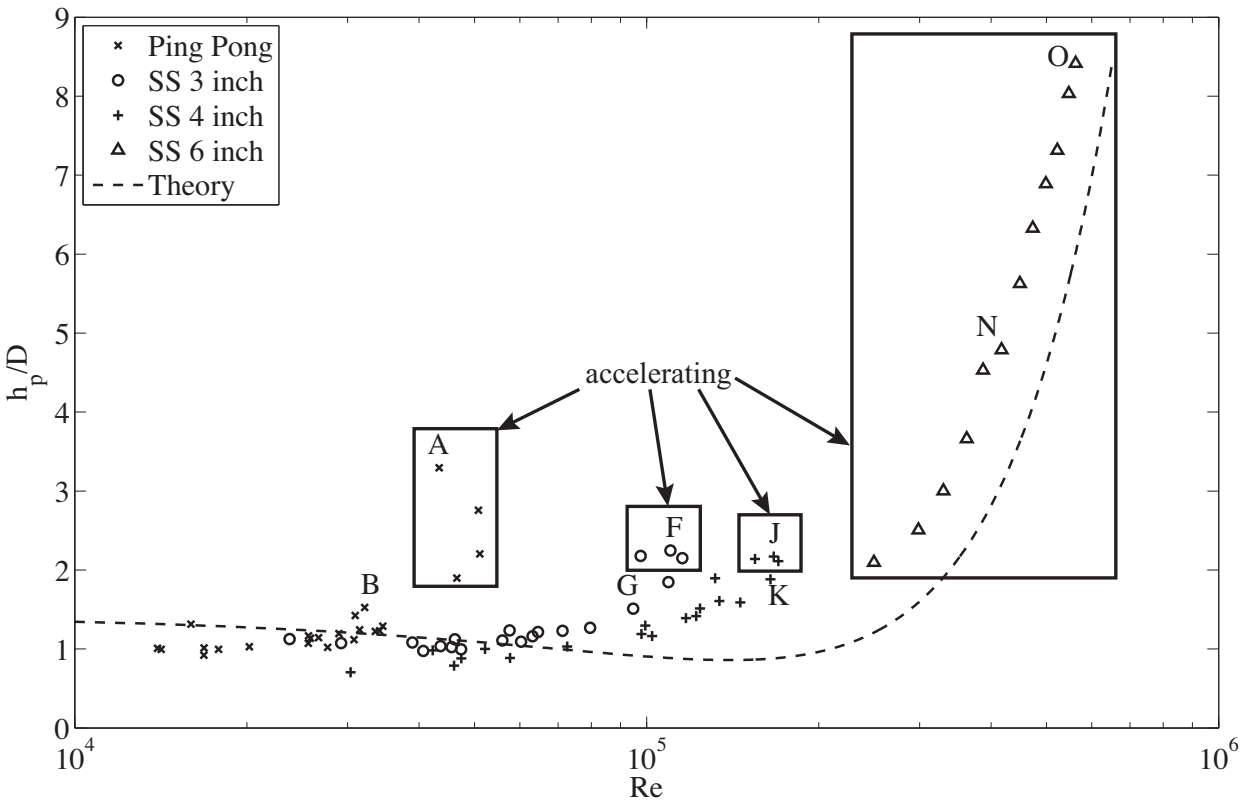

Figure 3.18: Re vs normalized popup height (h_p/D) for all spheres and release depths used in the present study.

A noticeable difference is seen between the *Re* and release depth, where deeper release depths for the SS6 case result in higher *Re* (cases N and O), and the other three spheres show greater *Re* from shallow release depths (cases A, F, G). This difference can again be attributed to the turbulent nature of the SS6 sphere with increased velocity and popup height as release depth increases. Whereas spheres rising in the laminar regime are affected by forces from vortex shedding which reduce velocity and popup height for spheres released from deep release depths. Another explanation for this difference comes from a comparison of the buoyancy (F_b) and drag forces (F_d). Buoyancy force increases as a cubed releationship with diameter (D) as follows

$$F_b = \frac{\rho \pi D^3 g}{6} \tag{3.2}$$

where the opposing drag force only increases as a squared relationship with diameter

$$F_d = 1/2\rho A C_d(Re)V^2$$
$$A = \frac{\pi D^2}{4} \tag{3.3}$$

Therefore, the buoyancy force dominates resulting a much greater exit velocity and h_p/D for the SS6 sphere with a greater diameter.

3.6 Low *Re*

As *Re* decreases, the ability of a sphere to overcome drag force and popup above the free surface enough to create separation decreases with lower *Re*. A 1.9 cm (0.75 inch) hollow aluminum sphere (m^* = 0.65) used in preliminary testing for selection of spheres to be used resulted in no significant popup above the free surface. The sphere exhibited an oscillatory trajectory during ascension underwater but failed to produce enough momentum to create separation from the free surface. The ball simply breached and skimmed across the free surface. A simple theoretical force balance gives good agreement to the preliminary results. Equation 1.3 yields a terminal velocity of 0.56 m/s ($Re = 9.44 \times 10^3$). Inserting the calculated velocity into equation 1.4, the maximum popup height (h_p) yields a normalized popup height (h_p/D) of 0.81. Therefore, the aluminum sphere will not separate from the surface of the water upon exit. It is possible for a sphere to achieve a greater popup height if the sphere breaches the free surface during the accelerating regime (shallower depths), however, preliminary tests did not yield any normalized popup height greater than 1 diameter for spheres with $Re < 9.44 \times 10^3$.

Other preliminary results showed that the use of hydrophobic coatings on all spheres change popup heights by only a fraction of a mm. Suggesting that the ability to shed water off of the sphere plays a very small role in the maximum popup height.

CHAPTER 4. CONCLUSION

We have shown the correlations between popup height and release depth and expounded upon regime definition through examination of accelerations and velocities at free surface exit. Trajectory of the spheres has been shown and our data and regime definition based upon trajectory agree with that of other scientists and past research. The repeatability of the acceleration and velocity at free surface exit and the resulting popup height is measured and shown with very small error.

Data have been reported for spheres in the laminar and turbulent regimes. For spheres rising in a laminar regime, shallow release depths produce the maximum accelerations and velocities at free surface exit resulting in the maximum possible popup heights. The maximum popup heights are a result of spheres exiting the free surface during the accelerating regime where the sphere reaches maximum velocity. An increase in release depth displays a decrease in popup height resulting from deceleration caused by a vortex shedding event. After reaching terminal velocity, spheres experience vortex shedding throughout the oscillatory regime resulting in unsteady accelerations and velocities at free surface exit. Following vortex shedding, the sphere accelerates resulting in an increase in popup height with further increased release depth. The popup height increases, never reaching the magnitude of first maximum height, until another vortex is formed and shed decreasing the popup height with increased release depth. This pattern of oscillating acceleration, velocity, and popup height is displayed for spheres with lower *Re*. For spheres rising in a turbulent regime (SS6), a linear increase in popup height with release depth is seen for the experiments completed in this study.

Vortex shedding events were captured via 2D PIV and the visualization described the event as expected. The vortices shed in the wake of the rising spheres affects the vertical acceleration and velocity. Vortex shedding occurs at regular intervals after release and affect the popup height directly.

Popup height plotted versus *Re* shows a predictable trend, wherein the theoretical values match the data well, except in the accelerating regime where the sphere popup height is higher as expected due to the greater acceleration and velocity at free surface exit.

The maximum popup height and deeper release depth behavior of the SS6 cases are incomplete due to our experimental constraints. However, these cases showed that spheres with large buoyancy to drag force ratios that have *Re* values near the turbulent transition can achieve heights much higher than predicted, indicating that the drag coefficient may be much lower in an accelerating, unsteady flow field. Future work will include continued experimentation at deeper depths of the SS6 sphere.

REFERENCES

[1] Bourrier, P., Guyon, E., and Jorre, J. P., 1984. "The 'pop off' effect: different regimes of a light ball in water." *European Journal of Physics,* **5**(4), p. 225. 1, 4, 17, 22, 25

[2] Hodges, G., 2012. "Emperor penguins: Escape velocity." *National Geographic*, November. 1

[3] Martin, R. A., Hammerschlag, N., Collier, R. S., and Fallows, C., 2005. "Predatory behaviour of white sharks (carcharodon carcharias) at seal island, south africa." *Journal of the Marine Biological Association of the United Kingdom,* **85**(05), p. 1121. 1

[4] Corkeron, P. J., 1995. "Humpback whales (megaptera novaeangliae) in hervey bay, queensland: behaviour and responses to whale-watching vessels." *Canadian Journal of Zoology,* **Vol. 73**, pp. 1290–1299. 1

[5] Bearzi, G., Politi, E., and di Sciara, G. N., 1999. "Diurnal behavior of free-ranging bottlenose dolphins in the kvarneri (northern adriatic sea)." *Marine Mammal Science,* **15**(4), pp. 1065–1097. 1

[6] Bettle, M. C., Gerber, A. G., and Watt, G. D., 2009. "Unsteady analysis of the six dof motion of a buoyantly rising submarine." *Computers & Fluids,* **38**(9), 10, pp. 1833–1849. 1

[7] Fidler, J. E., 1991. Venting apparatus for controlling missile underwater trajectory. 1

[8] Horowitz, M., and Williamson, C. H. K., 2010. "The effect of reynolds number on the dynamics and wakes of freely rising and falling spheres." *Journal of Fluid Mechanics,* **651**, p. 251. 3, 4, 5, 10, 25

[9] Newton, I., 1726. "Philosophia naturalis principia mathematica.". 4

[10] Karamanev, D. G., and Nikolov, L. N., 1992. "Free rising spheres do not obey newton's law for free settling." *AIChE Journal,* **38**(11), pp. 1843–1846. 4

[11] Karamanev, D. G., Chavarie, C., and Mayer, R. C., 1996. "Dynamics of the free rise of a light solid sphere in liquid." *AIChE Journal,* **42**(6), pp. 1789–1792. 4

[12] Jenny, M., Dušek, J., and Bouchet, G., 2004. "Instabilities and transition of a sphere falling or ascending freely in a newtonian fluid." *Journal of Fluid Mechanics,* **508**, p. 201. 4, 5, 14, 15, 25, 26

[13] Veldhuis, C. H. J., and Biesheuvel, A., 2007. "An experimental study of the regimes of motion of spheres falling or ascending freely in a newtonian fluid." *International Journal of Multiphase Flow,* **33**(10), 10, pp. 1074–1087. 4, 5, 25, 33

[14] Ern, P., Risso, F., Fabre, D., and Magnaudet, J., 2012. "Wake-induced oscillatory paths of bodies freely rising or falling in fluids." *Annual Review of Fluid Mechanics,* **44**, pp. 97–121. 5

[15] Wadell, H., 1935. "Volume, shape, and roundness of quartz particles." *The Journal of Geology,* **43**(3), April - May, pp. 250–280. 14

[16] Truscott, T. T., and Techet, A. H., 2009. "Water entry of spinning spheres." *Journal of Fluid Mechanics,* **625**(1), pp. 135–165. 15

[17] Horowitz, M., and Williamson, C. H. K., 2008. "Critical mass and a new periodic four-ring vortex wake mode for freely rising and falling spheres." *Physics of Fluids,* **20**(10), October, p. 101701. 33